

**Diagnostics for Single Ultrashort Laser
Pulses using Transient-Grating Frequency
Resolved Optical Gating (FROG)**

Diploma paper
by
Anders Sjögren

Lund Reports on Atomic Physics, LRAP-229
Lund, February 1998

Abstract

The subject for this work is laser pulse characterization. The technique studied, completely characterizes a single ultrashort laser pulse by giving the complex electric field. The technique is called Frequency Resolved Optical Gating (FROG). A prototype of the single shot Transient-Grating (TG) FROG is designed, assembled and experimentally evaluated. The FROG technique gives so called "FROG traces", from which significant qualitative laser-pulse information can be obtained visually. Only a single laser pulse is needed to create such a two-dimensional trace. Through a fast iterative algorithm the pulse can be completely, quantitatively characterized.

Table of contents

1	Introduction	5
1.1	For whom and why is pulse characterization interesting	6
1.2	General technique to measure “light-fast quantities”	6
1.3	Short laser pulses - characteristics and problems	8
1.4	The FROG in general	9
1.5	Development of phase and amplitude measuring techniques	10
2	The given conditions	11
3	Autocorrelators in theory and practice	13
3.1	Mathematical background	13
3.2	The idea behind autocorrelators in laser physics	13
3.3	The Second Harmonic Generation (SHG) autocorrelator used to measure pulse duration	15
3.4	Interferometric autocorrelators	18
3.5	The practical realization of an autocorrelator	18
4	The FROG in principle	19
4.1	Multi shot and single shot FROG	19
4.2	Phase retrieval algorithm	20
4.3	FROG trace characteristics	21
5	Designing of a FROG for the T³-laser system in Lund	22
5.1	Nonlinear processes and geometries	22
5.2	Conclusion	26
5.3	The single shot Transient Grating (TG) FROG in detail	26
6	Equipment	34
6.1	Light splitting and transport	34
6.2	Mirrors, beamsplitters, lenses, filters and optomechanical components	34
6.3	Nonlinear medium	35
6.4	Imaging spectrometer	36
6.5	CCD camera and controller	36
6.6	Computer and software	37
7	Experimental work	39
7.1	The TG FROG experimental setup	39
7.2	Secure alignment and optimization to get an undoubtable, true TG FROG signal	40
7.3	The IR sensitive camera	41
7.4	Alignment from day to day	41
7.5	Stray light	42
7.6	KDP - no good for FROG traces	42
7.7	TG FROG traces without the cylindrical lens	42
7.8	Multiple shot TG FROG	43
7.9	Changing the distance between the compression gratings	43
8	Results from experimental measurements	44
8.1	Single shot TG FROG	44
8.2	Multiple shot TG FROG	51
8.3	Conclusion - The Future FROG	52
8.4	Difficulties	52
8.5	Solutions	53
8.6	Acknowledgements	54
9	References	55

	4
Appendix A Derivation of relation between pulse duration and width of autocorrelation curve	58
Gaussian pulses	58
Sech pulses	59
Appendix B Additional nonlinear processes in the pulse alignment procedure	60
Appendix C Calibration of wavelength	61
Appendix D Calibration of delay	62
Appendix E Resolution of the delay-axis for TG FROG	62
Appendix F The PG FROG trace	63
Appendix G Chirp due to pulse propagation	65

1 Introduction

Any laser pulse has a minimal spectral width. The spectrum can be measured with a simple spectrometer, and the temporal profile with an autocorrelator. Given these measurements it is possible to determine if the pulse is as short as possible with the given spectrum. If it is, it is said to be Fourier Transform (FT) limited. If not, the pulse is non perfect. The reason why or in what way is impossible to determine with the given equipment. A non-perfect pulse does not have the same spectrum in every point of the temporal profile. An apparatus that could measure the spectrum for every temporal point, would indirectly give the complete pulse information. It would explain in what way the pulse is non perfect. Corrections could be made to improve the laser pulse. The task of this diploma work has been to construct and test a prototype of an apparatus that indirectly can measure the complex electric field, $E(t)$, of a single ultrashort laser pulse (≈ 100 fs). The complex electric field unambiguously characterize the laser pulse. It is calculated from a measured “trace” consisting of spectra from each and every different temporal point. The trace is aquired through the single shot Frequency Resolved Optical Gating (FROG) technique.

The atomic physics division at the Lund Institute of Technology is a part of Lund Laser Center (LLC), which includes many different laser systems used for research. The diploma work deals with one of these systems, namely the Table-Top Terawatt-laser (T³-laser), which was built in 1992 (Fig. 1.1). This laser has a repetition rate of 10 Hz, produces 100 fs long pulses¹ with about 200 mJ in each pulse.

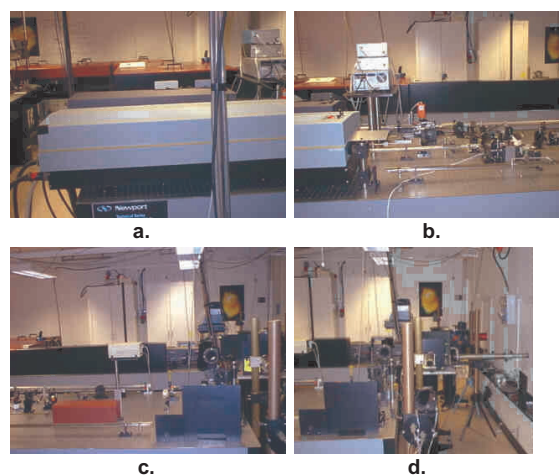


Figure 1.1. The T³-laser laboratory in Lund.

Presently, researchers demand not only intense laser pulses, but also a detailed characterization of each pulse. It is then possible to bind the experiments tighter to theories. The T³-system is today devoid of on-line, easy to use analysing equipment, which makes this diploma work an interesting subject, since it deals with pulse diagnostics.

¹ Full Width Half Maximum (FWHM) of intensity.

1.1 For whom and why is pulse characterization interesting

As the research using ultrashort lasers is diving deeper into the unknown, it is necessary to learn under what condition each experiment is done. Since laser pulses often constitute a major part of the experiments it is easy to understand why the need for laser pulse characterization increases rapidly. Up to now researchers have sometimes been forced to make the dangerous assumption that the laser pulse characteristics are known, without having the equipment to measure them. Of course, there has been ways to determine some characteristics of a laser pulse², but the complete picture has been missing.

In a number of experiments, for example high harmonic generation, X-ray generation and relativistic laser-electron interaction the laser pulse stands in the very center of attention. In all cases the pulse is focused to increase the intensity of the interacting light. Often it takes very high peak intensities and ideal experimental conditions to produce a measurable signal. A lot of time is spent optimizing parameters. If no proper laser diagnostic equipment is at hand, the main part of the experiment, the laser pulse, is neither characterized nor is it optimizable. It becomes more or less impossible to couple unexpected or absent results to the laser pulse. After many measurements the laser pulse might be pointed out as the unsolvable problem. At least if the right diagnostic equipment was not at hand.

All researchers using laser pulses need control of their laser equipment. Sometimes it is enough to know that the pulses look alike from day to day. Sometimes individual pulses must be fully characterized. The shorter and more intense the pulses become the more important pulse diagnostics become, but the diagnosing itself gets increasingly difficult.

1.2 General technique to measure “light-fast quantities”

Measuring light-fast quantities is problematic because light is travelling faster than anything else. But by using light itself to detect light it is possible to see light fast phenomena not as a function of time (which is impossible) but as a function of one, or many, spatial coordinates.

One simple example is a method to measure the period time, T , of a light wave using a Michelson interferometer (Fig. 1.2). For visible light, the magnitude of the period time is 10^{-15} seconds. Assume that a light wave enters the interferometer and is split in two. The two parts are recombined and the time average of the recombined signal intensity is measured. At the detector the E-fields of the two parts of the beam are mathematically expressed as

$$E_1(t) = E_2(t) = \frac{E_0}{2} \cdot \sin(\omega \cdot t). \quad (1.1)$$

The total intensity amplitude is measured,

$$I_{\text{detected}} \propto \langle E_1(t) + E_2(t) \rangle = \frac{E_0^2}{2}. \quad (1.2)$$

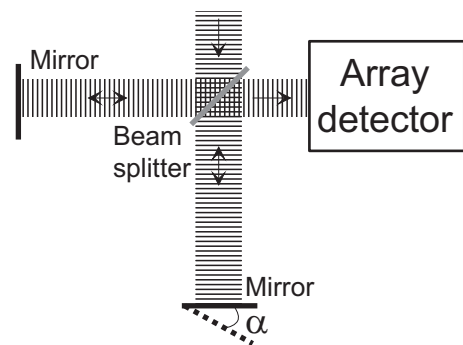


Figure 1.2. A Michelson interferometer setup.

² See the autocorrelation section.

One mirror is tilted a little bit³, α radians, so the second part of the light will not be in phase with the first part. The mathematical description is changed so that the phase of the second part depends on a spatial coordinate, x . The refractive index of air is n .

$$E_2(x, t) = \frac{E_0}{2} \cdot \sin\left(\omega \cdot t - x \cdot \frac{\omega}{c_0} \cdot n \cdot \sin(\alpha)\right) \quad (1.3)$$

The measured intensity changes accordingly,

$$I_{\text{detected}}(x) \propto \frac{E_0^2}{4} \cdot \left(1 + \cos\left(x \cdot \frac{\omega}{c_0} \cdot 2n \cdot \sin(\alpha)\right)\right) \quad (1.4)$$

A sinusoidal intensity pattern will form on the detector (Fig. 1.3). The period length (unit meter) depends on the angle α , which makes it possible to adjust the period length by tilting the mirror⁴. The measured period, L , is used to determine T .

$$T = \frac{2n \cdot \sin(\alpha)}{c_0} \cdot L \quad (1.5)$$

The method above is very exact, the only uncertainty being the angle, α , and the size of the detector. A very "fast quantity" has been made measurable through a arbitrarily high spatial frequency. The time dispersion in (1.5), $\Omega = \frac{2n \cdot \sin(\alpha)}{c_0}$, determines the relation between a spatial coordinate, L , and time, T . It will be further discussed later in the report.

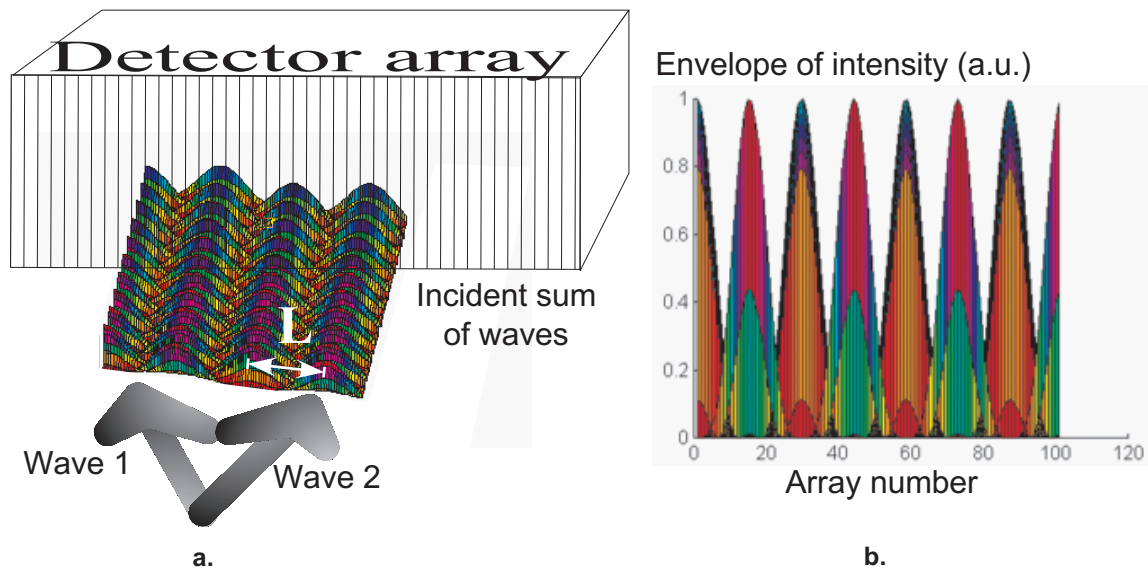


Figure 1.3. (a) The two incoming beams will create a sinusoidal intensity pattern when they overlap. (b) The sinusoidal pattern as the array detector sees it.

³ Actually it is the tiniest of tiny tiltings. The angle should be on the order of 10^{-3} degrees.

⁴ This makes the beams non-colinear, but the angle is small and the beams are assumed to have a large spatial cross section.

1.3 Short laser pulses - characteristics and problems

The classical Fourier transform, which is a purely mathematical manipulation, implies the same as the *Heisenberg Uncertainty Relation*, namely that

$$\Delta t \cdot \Delta f \geq \frac{1}{2\pi}. \quad (1.6)$$

In other words, the width of the frequency distribution affect the temporal duration and vice versa. Short laser pulses are very short in time so the frequency width must be large [1]. The interpretation is that short pulses consist of many frequencies, while long pulses may consist of only few frequencies. A continuous wave (CW) laser can have a very exact frequency, while a *100 fs* pulse must have a broad spectrum.

As shorter pulses are used in experiments, broad spectra become more important. Materials interact differently with different frequencies, and the temporal distribution of frequencies in the pulse, the *chirp*, becomes a question. A measured pulse spectrum does not give much information about the temporal profile of the pulse. That is because according to (1.6), $\Delta t \geq \frac{1}{2\pi\Delta f}$, and not $\Delta t = \frac{1}{2\pi\Delta f}$. The width of the spectrum, Δf ,

determines the shortest pulse duration possible, Δt , through the relation $\Delta t = \frac{1}{2\pi\Delta f}$. A

pulse fulfilling this equality is *transform limited* and is referred to as “perfect”. It has all its frequencies in every part of itself and is consequently devoid of chirp. A Gaussian, transform limited pulse may be written as

$$E(t) = E_0 \cdot e^{-a \cdot t^2} \cdot e^{i \cdot \omega_0 \cdot t}, \quad (1.7)$$

where $a = \frac{2 \cdot \ln(2)}{\tau_{FWHM}^2}$. The pulse temporal duration, τ_{FWHM} , will be referred to as simply

“pulse duration” throughout the report. It is the Full Width Half Maximum (FWHM) of the measured intensity profile,

$$I(t) \propto |E(t)|^2 = E_0^2 \cdot e^{-2a \cdot t^2}. \quad (1.8)$$

The fourier transform of (1.7) is the complex frequency profile,

$$\hat{E}(\omega) = \frac{E_0}{a} \cdot e^{-\frac{1}{4a}(\omega - \omega_0)^2}. \quad (1.9)$$

The squared absolute value of (1.9) is the the measured pulse spectrum,

$$|\hat{E}(\omega)|^2 = \left(\frac{E_0}{a}\right)^2 \cdot e^{-\frac{1}{2a}(\omega - \omega_0)^2}. \quad (1.10)$$

When a laser pulse is modified, the type of modification is important. The phase of the field can change,

$$E(t) = E_0 \cdot e^{-a \cdot t^2} \cdot e^{i \cdot \omega_0 \cdot t} \cdot e^{i \cdot \varphi_1(t)}, \quad (1.11)$$

which leads to a spectral change. Alternatively, the phase of different frequencies will change,

$$\hat{E}(\omega) = \frac{E_0}{a} \cdot e^{-\frac{1}{4a}(\omega - \omega_0)^2} \cdot e^{i \cdot \varphi_2(\omega - \omega_0)}, \quad (1.12)$$

which leads to a temporal change. An example of the first type of pulse modification is Self Phase Modulation (SPM). Different parts of the pulse “feel” different refractive indices (App. G). The second modification is for example Group Velocity Dispersion (GVD) (App. G). No matter what modification, a new complex temporal profile can be derived. If approximating that the new field is Gaussian, it becomes

$$E(t) = E_0 \cdot e^{-a' \cdot t^2} \cdot e^{i \cdot \varphi(t)}, \quad (1.13)$$

where $\varphi(t) = \varphi_0 + \omega_0 \cdot t + b \cdot t^2 + c \cdot t^3 + d \cdot t^4 + \dots$ and $a' \neq a$. The function $\varphi(t)$ is the complete phase of the manipulated pulse and φ_0 is an constant phase, ω_0 is the pulse carrier frequency and b , c and d is first order (linear), second order (quadratic) and third order (cubic) chirp. The instant frequency at a time, t , is $\frac{\partial \varphi(t)}{\partial t} = \omega_0 + 2b \cdot t + 3c \cdot t^2 + 4d \cdot t^3 + \dots$.

Consequently, if the chirp is linear, the frequency increases/decreases linearly as the pulse passes by.

If the phase is measured as a function of time the different orders of chirp can be calculated. It is then possible to adjust the laser to minimize the chirp. The shorter the pulse is, the larger the frequency difference of the front part and the end part may be. In research where ultra short pulses are used, a chirp may affect measurements in two ways. Either through elongation in time, or through the time varying frequency, or both.

1.4 The FROG in general

Autocorrelators will be a main issue in this report. It is because they are intimately coupled to the laser diagnosing tool called Frequency Resolved Optical Gating, or simply FROG. The phrase “optical gating” is a non-intuitive way of saying that light is used to measure light, or to gate the light to be measured. Only when all pulses are at the same place at the same time something happens. This is why the word “gating” is used. The pulses act as a gate to the signal. The gate opens only when all pulses overlap. “Optical gating” is also used in autocorrelators, discussed in Chapter 3, and in spectroscopic easurements [2,3].

“Frequency resolved” says simply that the signal is frequency resolved. The signal passes through a spectrometer or equivalent and its frequency components are distributed along a spatial coordinate.

1.5 Development of phase and amplitude⁵ measuring techniques

As new laser systems are developed, from the state of the art systems of the 1960:ies producing pulses with lengths down to 0.1 ns, to the systems of today giving pulses shorter than 10 fs, the need for new laser diagnostics has followed. First came methods that gave the pulse duration indirectly through theoretical reasoning and experimental measurements of for example second-harmonic-generation effectivity. Weber proposed a multiple shot autocorrelation measurement method already in 1966 [4], but it took until the 1970:ies before autocorrelation measurements were made experimentally [5,6]. When the streak cameras were developed in the 1980:ies, they were also used to measure pulse durations. Soon, however, the pulses were so short that not even streak cameras were fast enough. Even if the autocorrelation methods worked and were developed they did not suffice either. The reason is that short pulses have broad spectral widths, which allows the pulse duration to vary. It is difficult to tell whether the pulse is transform limited with just an autocorrelator. The only way to determine this is to measure the phase of the pulse as a function of time. A constant phase derivative versus time (or frequency) throughout the pulse means that the pulse is transform limited. During the 1980:ies researchers tried numerous methods [7-9]. The research was succesful and at the end of the decennium a few laboratories had measured both the complete E-field and phase as a function of time, mostly using a technique called Direct Optical Spectral Phase Measurement (DOSPM) [10-12]. Almost all teqniques required a steady flow of equivalent pulses coming from the laser. In the beginning of the 1990:ies, a new method were introduced by Daniel J. Kane and Rick Trebino⁶. They named it Frequency Resolved Optical Gating (FROG) [13-22]. The FROG immediately caught a lot of interest because of its simpleness. A FROG is in short an autocorrelator with an imaging spectrometer and a two dimensional detector added. After measurement (single shot or multiple shot), the FROG gives a so called FROG trace, from which the E-field and phase is retrieved through an iterative algorithm. Today FROG's are commercially available for many laser systems.

Even if the FROG is a very good diagnostic tool, the development towards alternative and/or better diagnostics continues. In France, for example, a research group at the research center Laboratoire d'Optique Appliquée (LOA) developes an alternative method, Cross-phase Modulation (XPM), to measure the phase and the E-field [23-25]. This method and a FROG will eventually both be in use to diagnose the T³-laser in Lund. The development of better FROGs also continues. Material studies in areas of optical communication and computing produce new materials with larger nonlinearities which contribute to the FROG development as well. The work of broadening the spectral region usable with FROG's is successfully continuing. Presently it is possible to analyse lasers at most wavelengths from the ultra violet (UV) region up to the middle infrared (IR) with the FROG [26].

It is worth mentioning that the birth of the FROG has in no way made normal autocorrelators superfluous. Instead, they have been put in the spotlight by FROG enthusiasts and are beeing developed even further. A simple second order autocorrelator using a simple geometry together with a third order FROG using a more complicated geometry, would meet many needs in a laser research laboratory of today.

⁵ The amplitude of the E-field.

⁶ Rick Trebino must be a busy man. His name seems to be appearing in most articles coming close to the FROG area.

2 The given conditions

For a successful accomplishment of the assignment it is important to have a clear picture of the given conditions. For the assignment the only presumption relates to the T³-laser.

Many articles have been written on T³-laser systems. One article discusses the T³-system in Lund and its first results [27], but the laser system has been much improved since the article was written. A low power laser pulse source delivers 100 fs pulses with correspondingly wide spectra. The pulses are temporally stretched about 3000 times by increasing their chirp. The chirp is created when the pulse passes two gratings. The pulses are amplified as much as possible without destroying the optics. After increasing the cross section they can be temporally recompressed with two other gratings, to very high power. The technique is called Chirped Pulse Amplification (CPA).

Now the system will deliver pulses with about 200 mJ energy. The pulse duration is about 100 fs, which corresponds to pulse powers of about 2 TW. The central wavelength is 800 nm and the repetition rate of the laser is 10 Hz.

By changing the distance of the compression gratings of the CPA system [27], the chirp is changed. One grating is fastened to a translator which is used to change the distance. A certain distance give pulses free from chirp, and therefore the shortest pulses. As seen in Figure 2.1 this corresponds to a translator reading of about 3.8 mm. At this position the pulses are presently about 110 fs. It is possible to produce 100 fs pulses if the laser setup is optimized. When doing multiple pulse autocorrelation experiments it is important that all pulses coming from the laser are almost equal (Ch. 3.3.1). On this system the pulse energy fluctuations can be 10%.

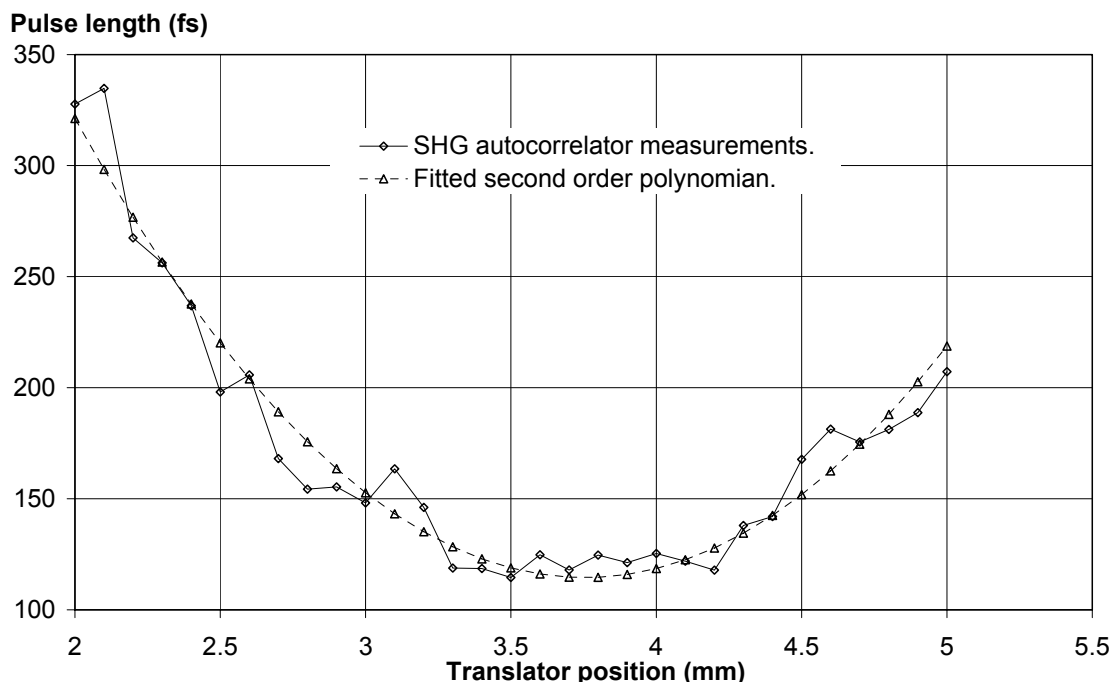


Figure 2.1. Pulse length as a function of grating distance.

The spectral frequency width of a Gaussian 110 fs pulse is

$$\Delta f_{\text{intensity FWHM}} = \frac{0.44}{\tau_{FWHM}} = 4.0 \quad \text{THz}, \quad (2.1)$$

which corresponds to a wavelength width of

$$\Delta \lambda_{\text{intensity FWHM}} = \frac{\lambda_0^2}{c_0} \cdot \Delta f_{\text{intensity FWHM}} = 8.5 \text{ nm}. \quad (2.2)$$

The wavelength width at 10^{-4} of the spectrum peak is about 30 nm .

The cross section of the laser pulse is assumed to be Gaussian in this report. It is probably more super Gaussian, but a Gaussian profile suffices as an approximation. A Gaussian FWHM cross section of about 24 mm is used in calculations in this report.

The polarization of the amplified laser pulse is linear horizontal.

The T³-system is currently beeing improved and upgraded. A part of the pulse ($\approx 20\%$) will be split off and amplified to about 10 TW . The power of the original system will be kept by increasing the original system amplification. Both systems will operate simultaneously.

Later on, further improvements will be made to the reduce pulse duration to 50 fs . This will double the power from the two systems, giving 4 TW and 20 TW respectively.

3 Autocorrelators in theory and practice

This chapter is important for the understanding of the report. It includes the foundation of nonlinear optics and it gives a beautiful recipe of how to make physics into mathematics and vice versa. Being the foundation of FROGs, the theory and practice of autocorrelators are of great importance.

3.1 Mathematical background

In mathematics, the expression

$$g(y) = \int_{-\infty}^{\infty} f(x)f(x+y)dx \quad (3.1)$$

is called the autocorrelation of $f(x)$. A cross correlation,

$$h(y) = \int_{-\infty}^{\infty} f(x)g(x+y)dx, \quad (3.2)$$

is more general and allows any two functions, $f(x)$ and $g(x)$. A convolution,

$$i(y) = \int_{-\infty}^{\infty} f(x)g(y-x)dx, \quad (3.3)$$

is very alike the cross correlation. In physics the expression

$$j(y) = \int_{-\infty}^{\infty} f^{n-1}(x)f(x-y)dx \quad (3.4)$$

is called the “ n :th order autocorrelation”, but it is, by definition, a type of cross correlation. As a reader of articles dealing with autocorrelators in physics, one should be aware of a certain confusion regarding the word ”autocorrelation”. In physics an ”autocorrelation” may in fact be a cross correlation, so mathematicians are easily misled. The correct mathematical definitions will be used throughout this report, although an autocorrelator will be called “autocorrelator” even if it is a cross correlator.

3.2 The idea behind autocorrelators in laser physics

Some basic concepts will be explained to clarify autocorrelator physics. It is important to understand what happens when many light pulses, or beams, overlap in media that are optically nonlinear. A material is optically nonlinear if the interaction between light waves and material is nonlinear. In fact, all medias are optically nonlinear, but in different ways. Assume that a laser pulse is split into two parts, and that they are made to overlap in a medium. The photons in the pulses will interact with the medium in some way. As an example the outer electrons of the atoms will try to follow the photons and therefore they will start to oscillate. It is important to remember that photons in a laser pulse are coherent. Therefore all photons from one pulse will cooperate in the interaction with the medium. If the two pulses accelerate the electron in different directions the pulses will affect each others environment and they will be coupled to each other through the medium. The most important interaction mechanisms are listed in Table 3.1. The response time indicates how fast a medium reacts to an E-field through a certain mechanism.

Table 3.1. Interaction mechanisms.

Mechanism	Response time (s)
<i>Electronic polarization</i>	10^{-15}
<i>Molecular orientation</i>	10^{-12}
<i>Electrostriction</i>	10^{-9}
<i>Saturated atomic absorption</i>	10^{-8}
<i>Thermal effects</i>	10^{-8}
<i>Photorefractive effect</i>	<i>intensity dependent</i>

Because of the coupling, the photons in the two pulses will scatter in different (well defined) directions and they may also change their oscillating frequency. Rules for scattering and frequency changing are derived by applying the conservation of momentum and energy.

A mathematical model will be presented that will explain what happens when optical pulses interact in a medium. It is extremely difficult to take into account the interaction between all photons and electrons. Therefore a pulse is treated not as a large number of individual photons, but rather as one oscillating electric field. In this approach the electric field of a laser pulse may look like this,

$$E(y, t) = \frac{E_0}{2} \cdot (e^{i(\omega_0 t - k \cdot y)} + e^{-i(\omega_0 t - k \cdot y)}) = E_0 \cdot \cos(\omega_0 \cdot t - k \cdot y). \quad (3.5)$$

Eq. (3.5) describes a continuous wave, not a pulse, but it can be viewed as part of a pulse. Calculations with this simplified expression are not so complicated and the results help to foresee the more complicated calculations for a real pulse. In fact, all information from the simpler calculation is also true for the more complicated one. If the more difficult problem is solved, more information would be the reward, but it would not contradict previous information.

The wave equation is well known to most physicists. It plays a central part in many physical phenomena. It is special because it looks essentially the same for waves of any kind. It tells for example what an electric field will look like as it is emitted from an oscillating electron. However, it is necessary to know which forces that act on the swinging object. The electron is affected by the photon and the atom it is bound to. The forces are very difficult to derive. Therefore the polarization, P , is introduced. It is a quantity that implicitly accounts for the forces acting on the electron. In short, the polarization describes the light-matter interaction. When an electron oscillates, due to an oscillating polarization, it will emit an electric field. The wave equation⁷,

$$\nabla^2 E(x, y, z, t) - \frac{n^2}{c_0^2} \cdot \frac{\partial^2 E(x, y, z, t)}{\partial t^2} = \frac{4\pi}{c_0^2} \cdot \frac{\partial^2 P(x, y, z, t)}{\partial t^2}, \quad (3.6)$$

is a linear differential equation. It gives the emitted electric field, E , as a function of the polarization, P . Although it looks difficult, the equation may be solved for many different polarizations. The polarization has to be calculated before the emitted E-field can be solved for.

Any function may be expressed as a polynomial with infinitely many terms. In reality only a couple of terms is enough for most purposes. The polarization is expressed as such a series,

$$P(x, y, z, t) = \chi^{(0)} + \chi^{(1)} \cdot E(x, y, z, t) + \chi^{(2)} \cdot E^2(x, y, z, t) + \chi^{(3)} \cdot E^3(x, y, z, t) + \dots \quad (3.7)$$

The polarization is a function of the electric field of the light pulses on one hand, $E(x, y, z, t)$, and on the atom and the atomic structure on the other, $\chi^{(i)}$ ⁸. Since $\chi^{(i)} < \chi^{(i+1)}$ the terms will get smaller and smaller. If the magnitude of the electric field is increased, however, the higher order terms will soon dominate. The right hand side of the wave equation includes the following expression,

$$\frac{\partial^2 P(x, y, z, t)}{\partial t^2} = \chi^{(1)} \cdot \frac{\partial^2 E(x, y, z, t)}{\partial t^2} + \chi^{(2)} \cdot \frac{\partial^2 E^2(x, y, z, t)}{\partial t^2} + \chi^{(3)} \cdot \frac{\partial^2 E^3(x, y, z, t)}{\partial t^2} + \dots \quad (3.8)$$

⁷ The equation is a bit simplified [13,14].

⁸ A tightly bound electron has small $\chi^{(i)}$.

The wave equation may be solved for each separate term in this expression. If a solution comes from the first order term, it is called a first order solution (or process⁹) and so on. If the signal created in an autocorrelator is due to a third order process, it is called a Third Order Autocorrelator (TOA) [28].

Numerical values of $\chi^{(i)}$ exist in tables and have been determined through experimental measurements [29,30]. That is because it is too difficult to calculate them even numerically.

3.3 The Second Harmonic Generation (SHG) autocorrelator used to measure pulse duration

The theory will now be used in practical laser physics. This is an example to show how a Second Harmonic Generation (SHG) autocorrelator may be used to measure pulse durations. It uses a second order process which doubles the frequency so it needs two separate pulses. Therefore the laser pulse is slit in two using a beamsplitter that reflects 50% of the intensity and transmits the other 50%¹⁰. The pulses overlap in a medium. The autocorrelation signal direction is along the bisector of the beam paths of the laser pulses. It is detected with some kind of light sensitive detector, preferably a CCD-chip. In the detector the signal energy is collected. In other words, the signal intensity is integrated with respect to time,

$$\text{Detected signal} = W_{sig} = \int_{-\infty}^{\infty} I_{sig}(t) \cdot dt . \quad (3.9)$$

The signal intensity for a SHG autocorrelator can easily be derived [31,32]. It is proportional to the product of the intensity profiles of the incoming pulses,

$$I_{sig}(t) \propto I_1(t) \cdot I_2(t) . \quad (3.10)$$

The detected signal is rewritten,

$$W_{sig} \propto \int_{-\infty}^{\infty} I_1(t) \cdot I_2(t) \cdot dt . \quad (3.11)$$

This expression is valid only if the two pulses that create the signal arrive in the medium at exactly the same time. If the second pulse is delayed by τ the expression is modified,

$$W_{sig}(\tau) \propto \int_{-\infty}^{\infty} I_1(t) \cdot I_2(t - \tau) \cdot dt . \quad (3.12)$$

The detected signal is a function of the delay. If the direction of delay is inverted, (3.12) changes to

$$W_{sig}(\tau) \propto \int_{-\infty}^{\infty} I_1(t) \cdot I_2(t + \tau) \cdot dt . \quad (3.13)$$

If the two pulses are identical, (3.13) becomes an autocorrelation of the intensity,

$$W_{sig}(\tau) \propto \int_{-\infty}^{\infty} I(t) \cdot I(t + \tau) \cdot dt . \quad (3.14)$$

⁹ Aiming at the process when the electron interacts with the photons.

¹⁰ It is not a demand that both pulses have the same intensity but it gives the strongest autocorrelation signal.

The detected signal will describe the autocorrelation of the pulse intensity profile as the delay of one pulse is changed (Fig. 3.1). A relation is derived in Appendix A that makes it possible to calculate the pulse duration from the width of the autocorrelation signal. Eq. (3.14) is identical to

$$W_{sig}(\tau) \propto \int_{-\infty}^{\infty} I(t) \cdot I(t-\tau) \cdot dt, \quad (3.15)$$

so the detected signal is the same which ever direction the delay has. The (SHG) autocorrelator will therefore always give a symmetric signal, from which it is impossible to tell if the pulse shape is unsymmetric.

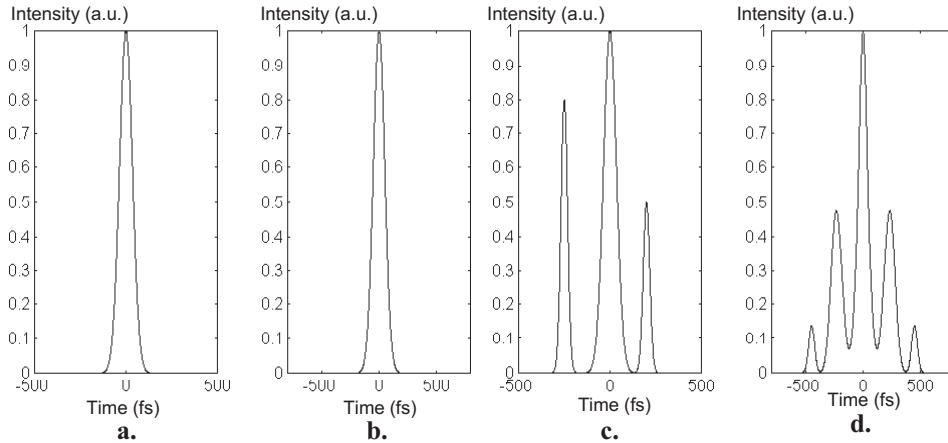


Figure 3.1. (a) A Gaussian pulse. (b) The autocorrelation of the pulse in (a). (c) A Gaussian pulse with a Gaussian sub-pulse. (d) The autocorrelation of the pulse in (c).

3.3.1 Multiple shot SHG autocorrelator

A multiple shot autocorrelator is characterized by colinear or nearly colinear incoming pulses focused with spherical optics (Fig. 3.2). If they are not colinear, it is important that the interpulse angle is as small as possible. Only then is (3.14) true. The beams would be colinear in a autocorrelator using a Michelson interferometer setup¹¹ but non-colinear for the more common setup in Figure 3.2. The signal intensity is measured for different delays of one pulse. The delay is always realized by moving mirrors in the autocorrelator setup. If the pulses to be measured are 100 fs the mirror must be moved with micron resolution about 100 μm in total.

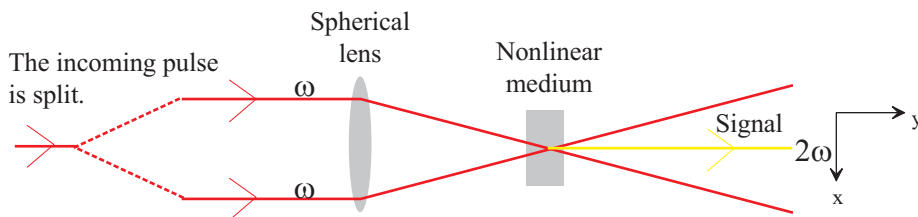


Figure 3.2. The principal multiple shot SHG autocorrelator setup.

¹¹ The variable delay is realized by moving one mirror back and forth.

The multishot autocorrelator is the easiest realizable type in a practical view. It has a number of drawbacks though. The major problem is that it demands many equal pulses from the laser. If the laser has a low repetition rate it will take long time to achieve a complete autocorrelation signal. Even if the repetition rate is high, the energy and/or pulse duration may change from pulse to pulse. This makes the signal fluctuate in time, which leads to a greater uncertainty regarding the duration of the pulse. The rather high demand on resolution when moving the mirror/s may also be a problem. Although translators with sufficiently high resolution exist they are expensive.

3.3.2 Single shot SHG autocorrelator

A single shot autocorrelator is characterized by non-colinear incoming pulses (Fig. 3.3). The delay varies along a spatial coordinate, just like in Chapter 1.2, and the whole autocorrelation signal is created with just one pulse from the laser. The signal is detected with an array detector resolving the delay axis to catch the whole autocorrelation curve in one shot. Figure 3.4 is a closeup of the overlapping incoming pulses. The size of the interaction region must not be too large compared to the diameter of the pulses. If it is, the cross section Gaussian profile will affect the signal. The direction of the signal is the bisector of the laser pulses [31,32]. The magnitude is a function of delay. In Figure 3.4, the delay varies along the x coordinate. To increase the signal strength cylindrical optics is frequently used. As seen by Figure 3.5 the signal is drawn out in the y -direction. By compressing the pulses in the x -coordinate direction the signal strength is increased without any loss of information.

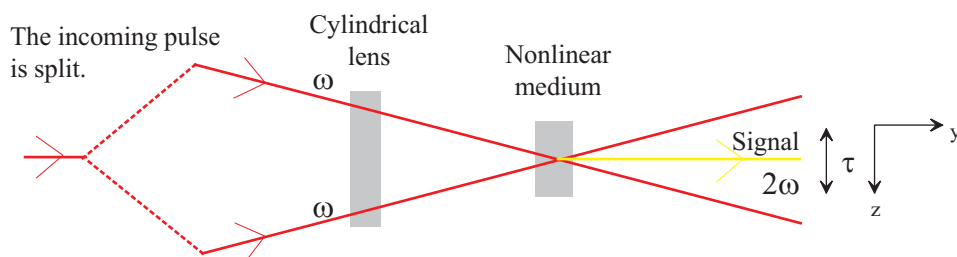


Figure 3.3. The principal single shot SHG autocorrelator setup.

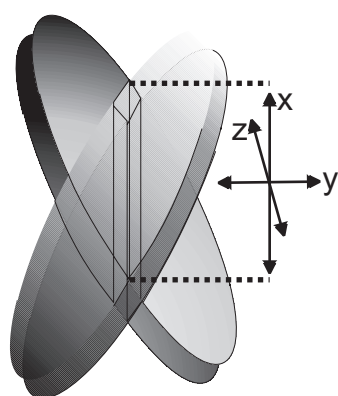


Figure 3.5. The signal is draw out in the x -direction.

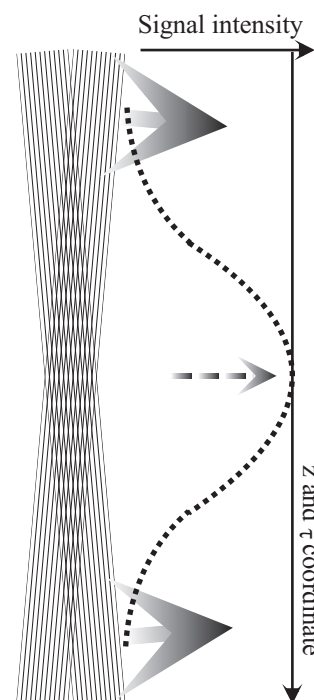


Figure 3.4. Two overlapping pulses and the SHG signal they may create in a nonlinear medium.

3.4 Interferometric autocorrelators

Interferometric autocorrelators are very interesting and do have a future, but in this report they are of minor importance. The only thing differing interferometric autocorrelators from the ones mentioned, so called slow autocorrelators, is that the resolution is better. Any slow autocorrelator may be converted to an interferometric autocorrelator by increasing the resolution. As an example the multiple shot Michelson SHG autocorrelator would become a interferometric autocorrelator if the signal could be detected with sub optical cycle resolution. If the resolution were this high the signal would be oscillating but have a curve like those in Figure 3.1 as an envelope. The oscillations are due to the optical cycles which are inherent in the oscillating phase of the light. In Chapter 1.2, in the beginning of the report, the duration of one optical cycle were measured. With some modifications the setup for that measurement can also be converted to an interferometric autocorrelator, perhaps a SHG autocorrelator.

As explained above, interferometric autocorrelators are sensitive to the phase to the light. They can be used to measure both E-field and phase as functions of time. Therefore an interferometric autocorrelator is an alternative to a FROG which measures the same quantities. The interferometric autocorrelator is a very sensitivity tool, but it is often difficult to realize one in a flexible laboratory environment that changes daily. The FROG is a much simpler alternative in a laboratory environment as it is more robust to changes. It is possible to realize single shot interferometric autocorrelators [33].

3.5 The practical realization of an autocorrelator

The possibilities are infinite. It all comes down to that one must be very sure of exactly what and how the autocorrelator should measure. The problem is the vast number of variables, such as those given in Table 3.2, must be optimized according to given conditions, such as those in Table 3.3. It is not an easy task to do this but it is not impossible.

Table 3.2. Variables

pulse intensity
pulse duration
spatial width of pulse
wavelength of pulse
spectral width of pulse
wavelength of signal
divergence of pulse
angles between pulses
polarization of pulses
polarization of signal
crystalline or non-crystalline
medium
orientation of crystal

Table 3.3. Conditions

background free signal
signal detector
single shot or multiple shot
measurement
repetition rate of laser

4 The FROG in principle

A FROG is easy to realize since little differs from existing autocorrelators. In fact, most autocorrelators are easily converted to a FROG by some add-on equipment. Specifically, the FROG frequency resolves the autocorrelation signal to receive a two dimensional intensity diagram with delay along one axis and wavelength along the other (Fig. 4.1). The wavelength dispersion is accomplished with a spectrometer or something equivalent. The delay dispersion is accomplished in two ways, depending on if it is a single shot or a multiple shot FROG (Ch. 4.3). The FROG trace is mathematically treated with an iterative algorithm called the *phase retrieval algorithm* to retrieve the actual E-field and phase of the laser pulse [14,34-36]. It is possible, however, to draw many conclusions about the laser pulse by just looking at a FROG trace, especially for an experienced FROG user.

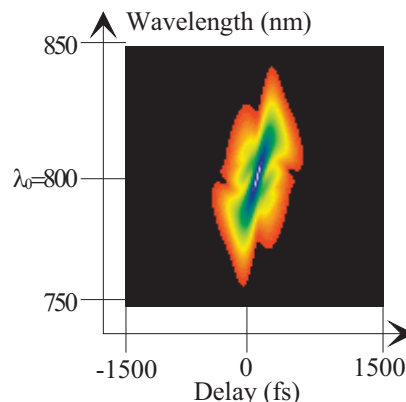


Figure 4.1. A Self Diffraction (SD) FROG trace for a pulse with heavy Self Phase Modulation (SPM) (App. G).

When using a FROG for the first time in a laser system, it might be good to run the algorithm to see what the pulse looks like, if it has any chirp etc. To achieve a nearly transform limited pulse it is almost always necessary to adjust something in the laser. After some work it should not be necessary to run the algorithm unless something is replaced or changed in the laser so that the pulse again becomes far from transform limited.

4.1 Multi shot and single shot FROG

Just as autocorrelators, FROGs may use multi shot or single shot geometries (setups). Because of the FROG, however, new autocorrelation geometries have been introduced and as a FROG designer, one has a lot of well investigated geometries to choose from. Naturally, the advantages and disadvantages of multi- and single shot geometries are the same as for autocorrelators (Ch. 3.3).

In multi shot FROG a spectrum of the signal is recorded for every delay step. All spectra are then put together to a FROG trace. In single shot FROG the signal already contains a delay axis. The input slit of an imaging spectrometer is aligned parallel to that axis as in Figure 4.2. At the output of the spectrometer the signal will exit as a complete FROG trace with delay along one axis, and wavelength along the other.

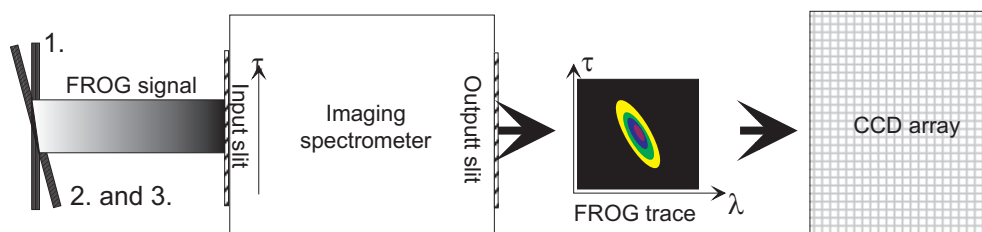


Figure 4.2. The created single shot FROG signal with the delay axis parallel to the input slit.

4.2 Phase retrieval algorithm

Once the FROG trace, $I_{FROG}(\omega, \tau)$, is experimentally recorded, the complex electric field, $E(t)$, is calculable. The phase retrieval algorithm used on FROG traces was originally not developed for FROG's. It solves a classical mathematical problem of retrieving a complex function from the amplitude of its two dimensional fourier transform. In the case of a one dimensional fourier transform this is impossible. The expression for a general FROG trace is the frequency resolved autocorrelation signal,

$$I_{FROG}^{SHG}(\omega, \tau) \propto \left| \int_{-\infty}^{\infty} E_{sig}^{FROG}(t, \tau) \cdot e^{-i\omega t} \cdot dt \right|^2. \quad (4.1)$$

Consider $E_{sig}^{FROG}(t, \Omega)$ to be the fourier transform of $E_{sig}^{FROG}(\omega, \tau)$ with respect to τ . Eq (4.1) is rewritten,

$$I_{FROG}^{SHG}(\omega, \tau) \propto \left| \int_{-\infty}^{\infty} \int_{-\infty}^{\infty} E_{sig}^{FROG}(t, \Omega) \cdot e^{-i\omega t} \cdot e^{-i\Omega \tau} \cdot dt d\Omega \right|^2. \quad (4.2)$$

If $I_{FROG}^{SHG}(\omega, \tau)$ is given and $E_{sig}^{FROG}(t, \Omega)$ is searched for, (4.2) is a two dimensional phase retrieval problem. When $E_{sig}^{FROG}(t, \Omega)$ is retrieved the complex electric field is

$$E(t) \propto E_{sig}^{FROG}(t, \Omega = 0). \quad (4.3)$$

Suppose $E_{sig}^{FROG}(t, \tau) \propto E(t) \cdot E(t - \tau)$ as for an SHG autocorrelator. Then we have

$$E_{sig}^{FROG}(t, \Omega = 0) = \int_{-\infty}^{\infty} E_{sig}^{FROG}(t, \tau) \cdot e^{-i \cdot 0 \cdot t} \cdot d\tau = \int_{-\infty}^{\infty} E(t) \cdot E(t - \tau) \cdot 1 \cdot d\tau \propto E(t). \quad (4.4)$$

It has been shown that existing phase retrieval algorithms almost always give unambiguous results for FROG traces [14,34,36].

4.3 FROG trace characteristics

When viewing a FROG trace it is possible to directly tell some things about the laser pulse (Fig. 4.3), without using the phase retrieval algorithm. The trace can be thought of as being a picture built up of spectra taken at different delays. That means, figuratively speaking, that separate signals are created at different delays, and each signal has a spectrum that is built of frequency components from the laser pulses interacting in the autocorrelation process. This is exactly true for multi shot FROGs but only true in principle for single shot FROGs. A signal at a large delay has a spectrum built of frequency components from approximately the end of the pulse and vice versa¹². If a laser pulse has a frequency distribution in time, so called chirp, the signals will have considerably different spectra. If the laser pulse has no chirp, the spectra will look the same for all delays (Fig. 4.3.a). The trace will be a straight ellipsis. It is analysed in Appendix F how traces for a certain type of FROG will look like if the pulse has a linear chirp. A linear chirp means that the mean frequency varies linearly with time (delay). Consequently the wavelength will vary approximately linearly with delay in the FROG traces of such pulses. The trace will therefore be a leaning ellipsis (Fig. 4.3.b). The larger the chirp, the larger the angle between the delay axis and the ellipsis. Figure 4.3.c shows a trace of a pulse with negative second order chirp of large amounts. This type of chirp leads to a wavelength increase for delays both larger and smaller than zero. In other words, the frequency is proportional to τ^2 . Figure 4.3.d is a trace of a pulse with positive linear and negative second order chirp. It is difficult to perceive the trace when the pulse has several different orders of chirp or has a strange time profile. Then the retrieval algorithm comes in handy.

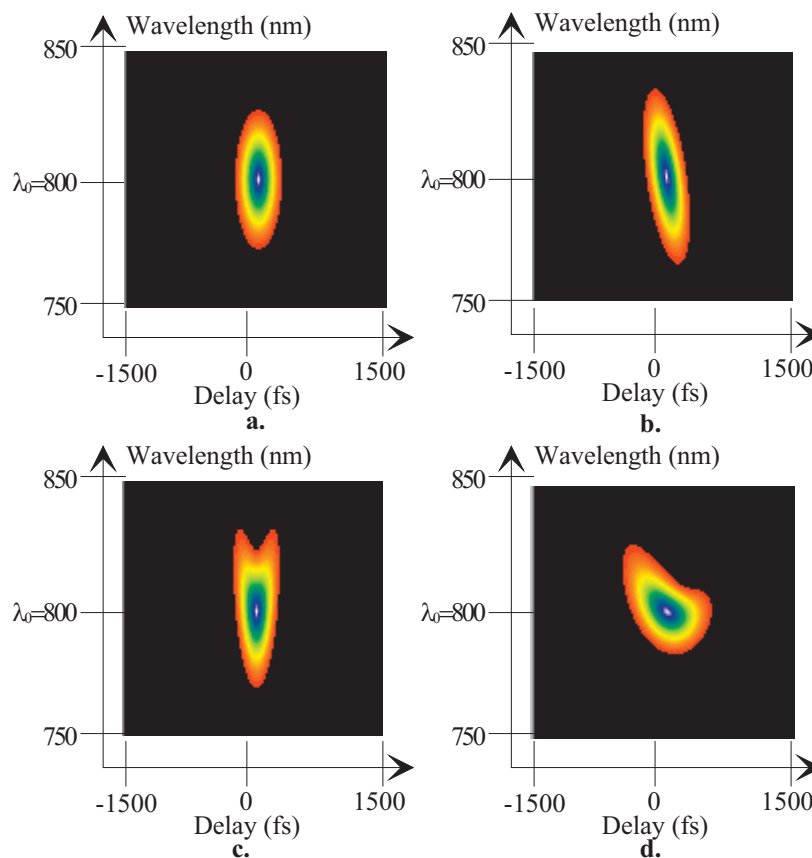


Figure 4.3. PG FROG traces of 110 fs pulses. (a) The pulse is transform limited. (b) The pulse has linear chirp. (c) The pulse has quadratic chirp. (d) The pulse has linear and quadratic chirp.

5 Designing of a FROG for the T^3 -laser system in Lund

Before a FROG can be assembled on an optical table necessary components must be ordered. With the purchase at hand a lot of decisions and calculations has to be done first, though.

5.1 Nonlinear processes and geometries

The foundation of a FROG is the autocorrelator. As known from the chapter on autocorrelators, the signal expression will look different depending on what kind of nonlinear process that is used. Each nonlinear process requires its own geometry. The number of required laser pulses also differs. The SHG autocorrelator (or SHG FROG) needs two pulses, but some third order processes require three pulses. Some nonlinear processes favors multi shot FROGs, some favors single shot FROGs, at least in a practical perspective.

As stated earlier there are many different processes and geometries which can be used for FROG. The processes and geometries of real interest are discussed here. The concluding chapter includes a table with a FROG geometry summary.

5.1.1 Second Harmonic Generation (SHG) FROG

This process and geometry is discussed in Chapter 3.3. One may achieve background free measurements with the non-collinear geometry. Because it is a second order process it is generally much more efficient than any third or higher order process. As all second order processes, however, it suffers from a major drawback. The FROG trace is always symmetrical with respect to delay even though the only truly symmetrical pulses are transform limited pulses. This ambiguity is made clear in Chapter 3.3. Figure 5.1 shows a SHG FROG trace for a double, non-symmetric laser pulse. A typical problem with the SHG FROG is phase matching [31,32]. The phase matching must be perfect or else the signal strength will not build up throughout the whole medium. Imperfect phase matching limits the medium thickness, and therefore also the signal strength. The expression for SHG FROG is

$$I_{FROG}^{SHG}(\omega, \tau) \propto \left| \int_{-\infty}^{\infty} E(t) \cdot E(t - \tau) \cdot e^{-i\omega t} \cdot dt \right|^2, \quad (5.1)$$

easily derived from eq (3.15). SHG FROG is easily implemented as a single shot geometry (Ch. 3.3).

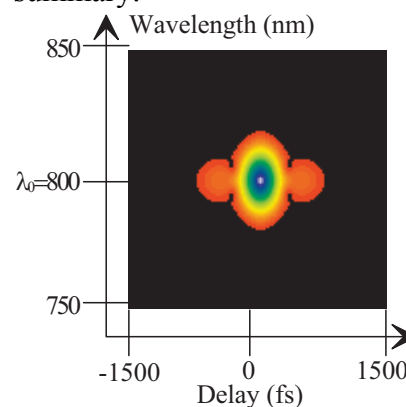


Figure 5.1. A SHG FROG trace for a double, non-symmetric, 110 fs pulse.

¹² This reasoning is correct depending on the type of FROG.

5.1.2 Third Harmonic Generation (THG) FROG

The setup is similar to the SHG FROG setup (Fig. 5.2). As the name implies, it is a third order process. The expression for THG FROG is [14]

$$I_{FROG}^{THG}(\omega, \tau) \propto \left| \int_{-\infty}^{\infty} E^2(t) \cdot E(t-\tau) \cdot e^{-i\omega t} \cdot dt \right|^2. \quad (5.2)$$

It is not as sensitive as SHG FROG but it has less delay ambiguity. That is, non-symmetrical pulse shapes mostly give non-symmetrical FROG traces. Figure 5.3 is a THG trace for a double pulse. Unfortunately, a pure linear chirp results in a symmetrical FROG trace. A special type of THG FROG, the Surface THG (STHG) FROG, is more sensitive than a normal THG FROG [37]. Because the nonlinear process is in this case the surface of the medium, phase matching is no problem. The STHG FROG has a large bandwidth as a result. Consequently, it may be used to measure pulses as short as a few femtoseconds. The THG FROG is usable as a single shot geometry.

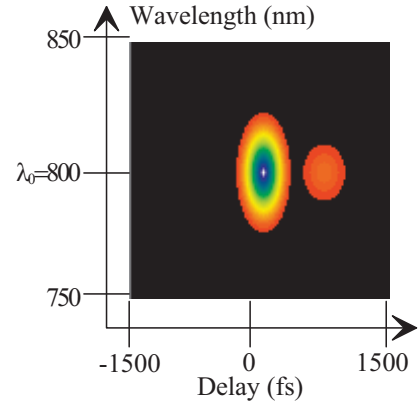


Figure 5.3. A THG FROG trace for a double, non-symmetric, 110 fs pulse.

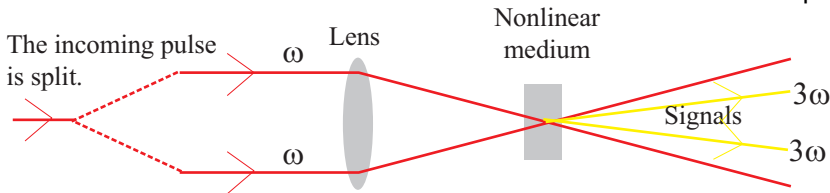


Figure 5.2. The THG FROG setup.

5.1.3 Polarization Gate (PG) FROG

This is a very popular type of FROG [38,39]. Figure 5.4 shows the geometry. The expression for the signal is [14]

$$I_{FROG}^{PG}(\omega, \tau) \propto \left| \int_{-\infty}^{\infty} E(t) \cdot |E(t-\tau)|^2 \cdot e^{-i\omega t} \cdot dt \right|^2. \quad (5.3)$$

It uses an automatically phase matched third order process using only two pulses. It is not very sensitive but the FROG traces are very intuitive and has no delay ambiguity (Fig. 4.3). A major disadvantage is the need of two broad band polarizers of very high quality. These are expensive, and if the quality is not good enough the signal to noise ratio quickly drops. The reason is evident in Figure 5.4. The signal is colinear with one of the laser pulses, but because it has opposite polarization, it is filtered out using a polarizer. Leakage of the laser pulse increases the background noise. PG FROG is easily turned into a single shot FROG.

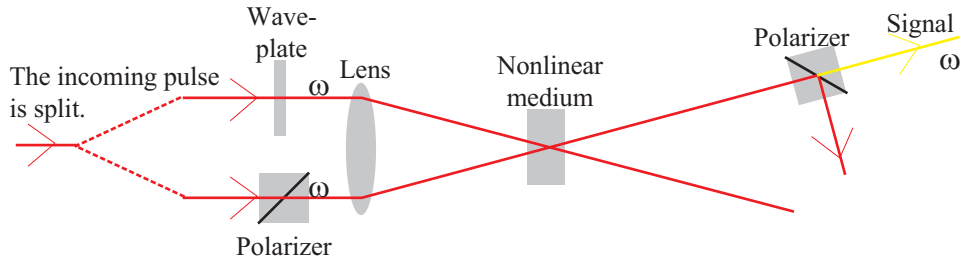


Figure 5.4. The PG FROG setup.

5.1.4 Self Diffraction (SD) FROG

This is a third order process not so often heard of (Fig. 5.5). Like PG FROG it is rather insensitive but has no delay ambiguities (Fig. 4.1). The process is not phase matched, so the medium must be very thin ($< 200 \mu\text{m}$) and the interbeam angle must be small ($< 2^\circ$). However, SD FROG is usable for UV pulses where good quality polarizers are almost unavailable. The expression for SD FROG is [14]

$$I_{FROG}^{SD}(\omega, \tau) \propto \left| \int_{-\infty}^{\infty} E^2(t) \cdot E(t - \tau)^* \cdot e^{-i\omega t} \cdot dt \right|^2. \quad (5.4)$$

SD FROG may be used to do single shot measurements.

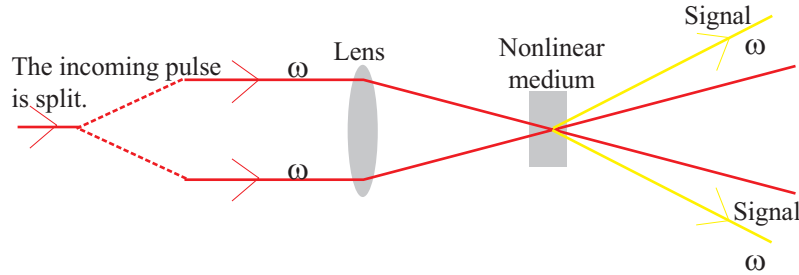


Figure 5.5. The SD FROG setup.

5.1.5 Transient Grating (TG) FROG

Being one of the latest geometries added to the FROG family it has experienced a lot of interest. The reason is that it is almost as sensitive¹³ as the SHG FROG and as intuitive as the PG FROG. In addition, it is background free and automatically phase matched. The geometry used for TG FROG is a boxcars geometry well known in nonlinear spectroscopy and in phase conjugation generation experiments (Fig. 5.6) [40,41]. Three pulses constitute three corners of a rectangle. The signal pulse goes through the fourth corner. The nonlinear process may be intuitively understood by thinking that two of the pulses, say one and two, creates a sinusoidal refractive index grating in the nonlinear medium on which the third pulse, number three, partially diffracts [31,32,42,43]. Because the TG geometry requires three beams, the signal has two different expressions. One is when only pulse two is delayed, and another when pulse one or three¹⁴ is delayed. The expression for the E-field of the signal is $E_{sig}(t) \propto E_1(t) \cdot E_2(t)^* \cdot E_3(t)$. If pulse number two is delayed this becomes $E_{sig}(t) \propto E_1(t) \cdot E_2(t - \tau)^* \cdot E_3(t)$. Since all three pulses are identical the FROG signal is identical to the SD FROG trace.

¹³ Because it uses a on diagonal element of the third order susceptibility tensor.

¹⁴ Because of symmetry it doesn't matter which one.

$$I_{FROG}^{TG2}(\omega, \tau) = I_{FROG}^{SD}(\omega, \tau) \propto \left| \int_{-\infty}^{\infty} E^2(t) \cdot E(t-\tau)^* \cdot e^{-i\omega t} \cdot dt \right|^2 \quad (5.5)$$

If, on the other hand, pulse one or three is delayed the signal E-field is $E_{sig}(t) \propto E(t-\tau) \cdot |E(t)|^2$. Through a change of variables and a change of symbols this becomes $E_{sig}(t) \propto E(t) \cdot |E(t+\tau)|^2$, which is the E-field of the PG FROG but with a reversed sign of the delay. The expression for this signal is

$$I_{FROG}^{TG1,3}(\omega, \tau) = I_{FROG}^{PG}(\omega, -\tau) \propto \left| \int_{-\infty}^{\infty} E(t) \cdot |E(t+\tau)|^2 \cdot e^{-i\omega t} \cdot dt \right|^2. \quad (5.6)$$

The TG FROG yields SD or PG FROG traces as given in Figure 4.1 and 4.3. Sweetser, Fittinghoff and Trebino states that it should be possible to realize a single shot TG FROG [16]. However, Sweetser states that, to the best of his knowledge, no experiments with a single shot TG FROG have been done, and that "... there are some subtleties involved with it..." [44].

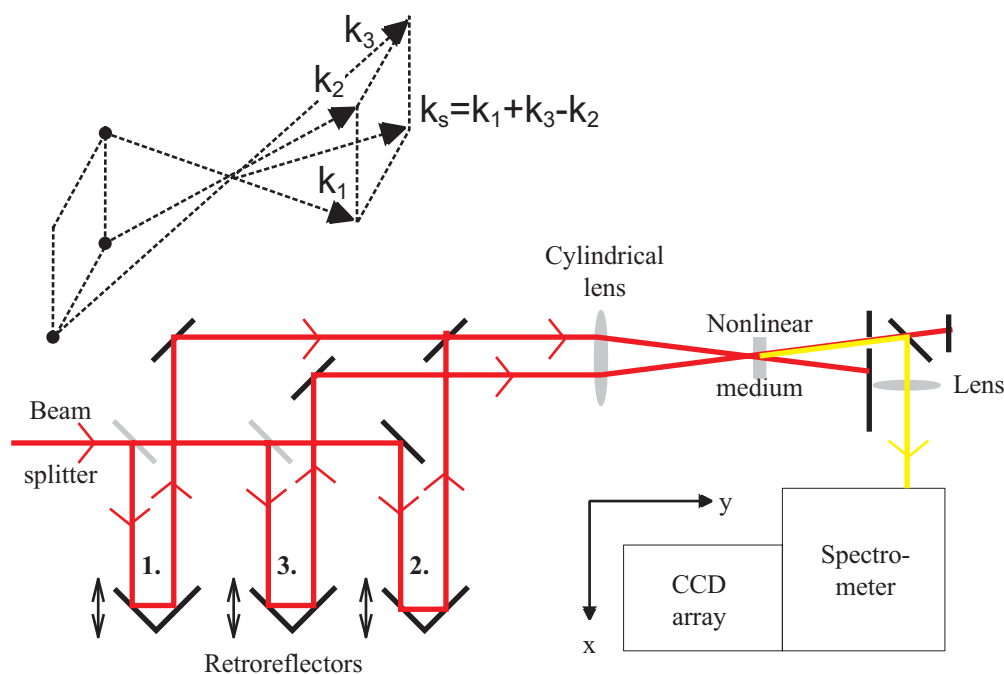


Figure 5.6. (a) The TG FROG setup and the phase matching condition defining the signal direction.

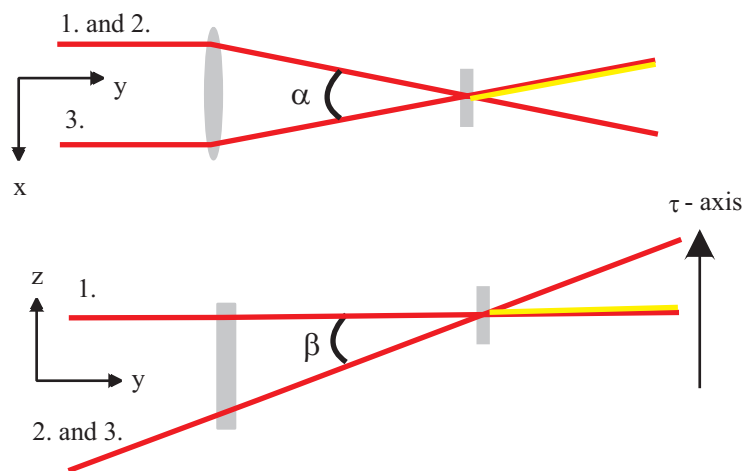


Figure 5.6. (b) The TG signal creation viewed from two directions.

5.2 Conclusion

Table 5.1 summarizes the different FROGs. By looking at it the SHG and THG FROGs are disregarded because of their ambiguities and unintuitive traces. SD is problematic because it requires a very thin medium. PG also suffers from a special requirement and it is not background free. But the TG FROG gives the same intuitive signals as PG or SD FROGs and is more sensitive as well. Therefore it was decided to use the single shot TG FROG for characterization of the Lund T³-system.

Table 5.1. Summary table of FROG characteristics.

Geometry	SHG	THG	PG	SD	TG
Nonlinearity	<i>Second order</i>	<i>Third order</i>	<i>Third order</i>	<i>Third order</i>	<i>Third order</i>
Sensitivity (single shot)	<i>~0.01 μJ</i>	<i>~0.03 μJ</i>	<i>~1 μJ</i>	<i>~10 μJ</i>	<i>~0.1 μJ</i>
Sensitivity (multi shot)	<i>~0.001 nJ</i>	<i>~3 nJ</i>	<i>~100 nJ</i>	<i>~1000 nJ</i>	<i>~10 nJ</i>
Advantages	<i>Very sensitive, background free</i>	<i>Sensitive, very large bandwidth, background free</i>	<i>Intuitive traces, automatic phase matching</i>	<i>Intuitive traces, background free</i>	<i>Background free, sensitive, intuitive traces, automatic phase matching</i>
Disadvantages	<i>Unintuitive traces</i>	<i>Unintuitive traces</i>	<i>Requires polarizers</i>	<i>Requires thin medium, not phase matched</i>	<i>Three beams</i>
Ambiguities	<i>Direction of time, relative phase of multiple pulses</i>	<i>Relative phase of multiple pulses</i>	<i>None known</i>	<i>None known</i>	<i>None known</i>

5.3 The single shot Transient Grating (TG) FROG in detail

So far, the theory and practice regarding the TG FROG has been only briefly introduced. The following section will give a more complete picture.

5.3.1 Nonlinear medium

To create a TG signal, a suitable nonlinear medium is necessary. Specifically, such a medium has non-zero on-diagonal elements of the third order susceptibility, $\chi^{(3)}$ (Ch. 3.2) [31,32,40,41]. However, if the medium is crystalline that is not the only requirement. Because the laser pulses traverse the medium at different angles relative to the crystal axis/axes, differently polarized light may "feel" different refractive indices. This will result in an undesirable prolongation of the pulses. Therefore no birefringent¹⁵ crystalline medium should be used. In articles treating TG FROG only amorphous (non-crystalline) SiO₂, quartz, is mentioned. Because the response is mainly through the photorefractive effect one does not need to worry about the response time.

¹⁵ A term telling that light with two different polarizations "feels" two different refractive indices.

5.3.2 A theoretical analysis of the delay dispersion

Any single shot geometry converts time (delay) into a spatial coordinate. The magnitude of the delay dispersion is very important in single shot FROG measurements. In multi shot FROG's the delay is easy to control. By moving a translation stage the spatial delay, Δx , of one pulse is varied. The spatial delay is easily converted to a time delay, $\tau = 2 \cdot \frac{\Delta x}{c}$ s. Each position of the translation stage

correspond to a delay. By recording a spectrum for the signal at different delays a complete FROG trace is achieved. If the delay step between adjacent signal recordings is large the delay dispersion is large. Also, if the delay step is large the delay sampling rate is low. Few recordings must be done to cover the whole temporal pulse shape. With small time steps the delay dispersion is small and the sampling rate is high, but many more recordings has to be done.

In single shot FROG, however, where the signal already contain a delay axis, questions arise regarding the delay dispersion. As the single shot FROG trace is recorded, preferably with a CCD camera, the trace will be put on a lattice of pixels. The delay time between adjacent pixels, the delay dispersion, must be calculated theoretically.

Consider the three crossing beams of spatial length $a = \frac{c_0}{n_{\text{medium}}} \cdot \tau_{\text{FWHM}}$ in the medium (Fig. 5.7).

It may not be obvious why it is possible to view the interaction region in two dimensions since the pulses in fact traverses in three dimensions. The reason is, as will be evident below, the cylindrical lens. With simple geometrics, the length of the interaction region, H , is derived as a function of the interpulse angle, β ,

$$H(\beta) = a \cdot \tan\left(\frac{\beta}{2}\right) + \frac{2a}{\tan(\beta)} \approx \frac{2a}{\tan(\beta)} = \frac{2c_0}{n_{\text{medium}} \cdot \tan(\beta)} \cdot \tau_{\text{FWHM}} \quad (5.7)$$

At the upper part of the interaction region pulse two and three are delayed by τ_{FWHM} and at the lower part they are delayed by $-\tau_{\text{FWHM}}$. The delay dispersion is

$$T = \frac{2\tau_{\text{FWHM}}}{H(\beta)} = \frac{n_{\text{medium}} \cdot \tan(\beta)}{c_0} \quad (5.8)$$

If the angle is $\beta = 3.73^\circ$ and the refractive index $n_{\text{medium}} = 1.51$, the delay dispersion is

$$T = 328 \frac{\text{ps}}{\text{m}} = 7.88 \frac{\text{fs}}{\text{pixel}} \quad (5.9)$$

The latter delay dispersion is calculated because the detector pixel spacing is $24 \mu\text{m}$.

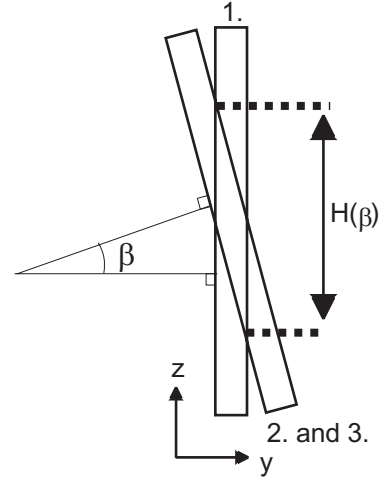


Figure 5.7. The region where the three pulses overlap.

5.3.3 The trace of the single shot TG FROG

TG FROG may yield traces identical to the traces obtained with PG or SD FROG depending on which pulse is delayed. But in a single shot geometry no pulse is delayed. At least not in the usual sense. Instead the delay is realized by the interpulse angle (Fig. 5.7). The type of FROG trace is in this case determined by the orientation of the cylindrical lens. It is possible to orient the cylindrical lens in three ways and get a true TG FROG signal (Fig. 5.8).

The input slit of the spectrometer must be oriented accordingly. Position A and C yield PG FROG traces, because pulse one or three are delayed. Position B yields SD FROG traces because pulse two is delayed. The cylindrical lenses may be removed. Nothing happens except that the pulses are not focused when interacting (Fig. 3.5), so the signal strength drops. Still, the slit positions in Figure 5.8 will yield the same traces. The assembled TG FROG of this project gives PG traces, with or without the lens.

Suppose cylindrical lenses are used and that the spectrometer input slit and lens is in position A (Fig. 5.9). The direction of positive delay must be figured out. When moving along the z -axis in negative direction, pulse one is increasingly delayed with respect to the other two pulses. Consequently, the delay axis for the expression in eq 5.6 is directed opposite to the z -axis.

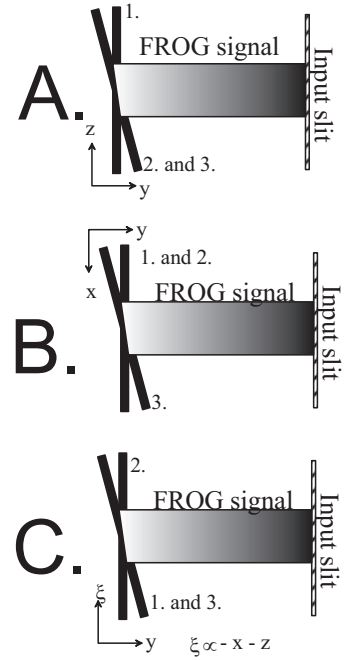


Figure 5.8. The three ways to orient the cylindrical lens and the spectrometer input slit.

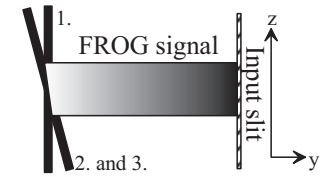


Figure 5.9. The direction of the delay axis.

5.3.4 The resolution of the delay axis

The delay resolution is an important subject in FROG measurements. Because the interaction region, the region where all three beams interact, moves through the medium, the origin of the signal moves. A part of this movement is along the delay axis. This implies that the delay axis of the trace will be smeared and that the resolution will be reduced. In Appendix E, an expression for the delay resolution is derived to be

$$\Delta \tau = \frac{n_{\text{medium}} \cdot d}{c_0} \cdot \tan\left(\frac{\beta}{2}\right) \cdot \tan(\beta) \approx \frac{n_{\text{medium}} \cdot d}{c_0} \cdot \frac{\beta^2}{2}, \quad (5.10)$$

where d is the thickness of the nonlinear medium.

5.3.5 The delay axis of the FROG trace

The angle, β , in Figure 5.6 determines the delay dispersion. A small angle results in a low delay dispersion on one hand, which is preferable. On the other hand the size of the FROG trace increases in the delay direction as the delay dispersion is lowered. Because the height of the input and output of the spectrometer limits the size of the trace in delay direction, the delay dispersion cannot be arbitrarily low. The highest dispersion depends on the pulse duration and temporal profile complexity. A FROG trace is usually regarded as complete (not cut) when all structures, four orders of magnitude lower than the peak are included [35]. For any third order FROG, this implies, through a simple calculation, that the total delay for third order traces must be at least

$$\tau_{\text{total delay}} \geq \sqrt{\frac{6 \cdot \ln(10)}{\ln(2)}} \cdot \tau_{\text{FWHM}} \approx 4.5 \cdot \tau_{\text{FWHM}}. \quad (5.11)$$

Taking into account the total magnification of the trace along the delay axis for the present setup, it is possible to calculate the spatial length of the delay axis as the trace exits the spectrometer. This is done for a transform limited 100 fs pulse for different values of the angle β in Table 5.2.

Table 5.2. Size of delay axis after spectrometer at $I_{\text{FROG}}(\omega, \tau) / I_{\text{FROG}}^{\text{peak}} = 10^{-4}$.

Angle β (°)	Delay dispersion (ps/m)	Delay resolution for $d=1$ mm (fs)	Spatial length at output slit (mm)
$\beta_{\min}=0.44$	$T_{\min}=39$	0.15	7.0
0.93	82	0.7	5.5
2	176	3.1	2.5
3	264	6.9	1.7
3.73	328	11	1.4

The vertical size of the output is 7 mm for the present spectrometer, so the smallest angle is $\beta_{\min}=0.44^\circ$ leading to a delay dispersion of $T_{\min}=39$ ps/m. Presently, the FROG trace is magnified m times by the spectrometer and the objective, see Appendix D, the delay dispersion, T , changes,

$$T_{\text{at CCD chip}} = \frac{T_{\text{at nonlinear medium}}}{m}. \quad (5.12)$$

The trace is recorded on a CCD chip with pixels of size $24 \times 24 \mu\text{m}$ (Ch. 7.5). The pixel size, eq (E.6) and the magnification is what limits the delay resolution. Up to the angle

$$\beta_{\text{critical}} = 2 \cdot \arctan\left(\frac{24 \cdot 10^{-6}}{m \cdot d}\right) \quad (5.13)$$

the delay resolution is lower than the pixel size, so only the pixel size limits the resolution. Only magnification, m , and medium thickness, d , affects this angle. The angle for different medium thicknesses is listed in Table 5.3. It is favorable to use angles smaller than β_{critical} .

Table 5.3. β_{critical} for different medium thicknesses with $m=0.608$.

d (mm)	β_{critical} (°)
0.55	8.2
0.75	6.0
1	4.5

5.3.6 The marginals

The marginals of a FROG trace are defined as

$$M_{\tau}(\tau) = \int_{-\infty}^{\infty} I_{FROG}(\omega, \tau) \cdot d\omega, \quad (5.14)$$

which is the delay marginal, and

$$M_{\omega}(\omega) = \int_{-\infty}^{\infty} I_{FROG}(\omega, \tau) \cdot d\tau, \quad (5.15)$$

which is the frequency marginal. Depending on the type of FROG trace, it can be possible to measure and calculate the marginals with help of an autocorrelator and different spectra of a laser pulse [35,17]. Therefore they serve as powerful consistency checks. In Appendix F, the expression for the delay marginal for PG FROG,

$$M_{\tau}^{PG}(\tau) \propto \int_{-\infty}^{\infty} I^2(t) \cdot I(t-\tau) \cdot dt, \quad (5.16)$$

which is a third order cross correlation, is made plausible. With help of eq (5.16) and (A.5) the approximate pulse duration can be calculated. As stated in Appendix F, the PG frequency marginal is

$$M_{\omega}^{PG}(\omega) \propto I(\omega) \cdot F\left(\int_{-\infty}^{\infty} I(t) \cdot I(t-\tau) \cdot dt\right). \quad (5.17)$$

When the results from FROG measurements are doubtful, or at any time, the marginals can rule out problems with the FROG itself and point out that the problem is the laser, or opposite.

5.3.7 An important limitation

All FROG traces must be analysable with the iterative retrieval algorithm. Since the algorithm uses the Fast Fourier Transform (FFT), each trace will be rescaled to fit a time-frequency grid ideal for the transformations. Because of this the step length in delay and frequency has a predetermined general relation,

$$\Delta\tau \cdot \Delta f = \frac{1}{N}, \quad (5.18)$$

where $N \times N$ is the size of the grid. The delay step length must be large enough so the FROG trace don't extend off the grid in the delay direction. From eq (5.11) this demand can be found for PG traces,

$$\Delta\tau \geq \frac{\sqrt{\frac{6 \cdot \ln(10)}{\ln(2)}}}{N} \cdot \tau_{FWHM} \approx \frac{4.5}{N} \cdot \tau_{FWHM}. \quad (5.19)$$

Equally, the frequency step must be such that the FROG trace don't extend off the grid in frequency direction. Eq (F.2), which holds for PG traces, leads to

$$\Delta f \geq \frac{\sqrt{\frac{12 \cdot \ln(10)}{\ln(2)}}}{N} \cdot f_{FWHM} \approx \frac{6.3}{N} \cdot f_{FWHM} \Leftrightarrow \quad (5.20)$$

$$\Delta f \geq \frac{\sqrt{\frac{12 \cdot \ln(10)}{\ln(2)}} \cdot c_0}{N \cdot \lambda_0^2} \cdot \lambda_{FWHM}$$

Eq (5.20) is rewritten with help of (5.18),

$$\Delta\tau \leq \frac{\lambda_0^2}{\sqrt{\frac{12 \cdot \ln(10)}{\ln(2)}} \cdot c_0 \cdot \lambda_{\text{FWHM}}}. \quad (5.21)$$

Now there are two conditions placed on the delay step for PG traces. The first is (5.19) and the second is (5.21). For a transform limited pulse, 100 fs at 800 nm, the conditions are

$$\begin{aligned} 7.0 \text{ fs} \leq \Delta\tau \leq 36 \text{ fs}, \quad N = 64 \\ 3.5 \text{ fs} \leq \Delta\tau \leq 36 \text{ fs}, \quad N = 128 \end{aligned} \quad (5.22)$$

for two different grid sizes. The delay step conditions can be transformed into β angle conditions for TG FROG, because the angle determines the delay dispersion, which together with the magnification and pixel size determines the delay step. The corresponding conditions on the angle are for TG FROG

$$\begin{aligned} 2.0^\circ \leq \beta \leq 10^\circ, \quad N = 64 \\ 1.0^\circ \leq \beta \leq 10^\circ, \quad N = 128 \end{aligned} \quad (5.23)$$

It is important to compare these conditions with β_{\min} and β_{critical} to see which angle interval that is permitted.

5.3.8 Simulations of the TG FROG

A number of simulations has been done either to verify theoretical results or to calculate the magnitude of unwanted phenomena. The simulations quantitatively regard the special case of the present TG FROG setup, but they hold qualitatively for any autocorrelation.

i. Delay dispersion

The deduction of the delay dispersion is very important since it defines the delay axis of the FROG trace. The simpleness of the geometrical deduction is worrying. Some simulations of the process will tell if the deduction is correct.

The amplitude of a Gaussian pulse in two dimensions with the wave vector, \square , is

$$\left| E_i^{\text{laser pulse}}(x, y, t) \right| \propto e^{-2 \cdot \ln(2) \cdot v^2 \cdot \left(\frac{\vec{k}_i \cdot (x, y)}{\tau_{\text{intensity FWHM}}} \right)^2}. \quad (5.24)$$

Simply multiplying three such pulses with each other will give a picture of the interaction region in two dimensions if the pulses have appropriate directions. Squaring and integrating the interaction region in the direction of the signal, yields a curve that is proportional to the detected intensity of the signal. The simulation verifies the calculated delay dispersion for the TG traces even better than expected.

ii. The delay smearing effect

The delay smearing that limits the delay resolution, could theoretically induce a broadening of the signal in delay direction. The same simulation as above is done but with the delay smearing incorporated. Through the simulations it is clear that the smearing do not affect the width of the signal by more than 1% for reasonable angles and material thicknesses. Broadening due to the smearing may consequently be neglected in the present TG FROG setup.

iii. The divergence of the FROG signal

Short pulses with broad spectra may give divergent autocorrelation signals, which will lead to a magnification of pulse duration and reduce the delay resolution. The reason is that as the pulses interact, different frequencies interact with each other. The frequencies of the beams determine the direction of the signal. When different frequencies interact they will give rise to signals travelling in slightly different directions. The “should be” signal direction is determined by the central frequency. It would be interesting to know how big this problem is.

A condition to make the simulation reasonably easy is that the laser pulses are transform limited, which makes it possible to say that all frequencies are in all points of each pulse. The simulation program combines all frequencies of the three beams to get all possible directions and simultaneously calculates the probability that each frequency mix will occur. The directions together with the probabilities are used to

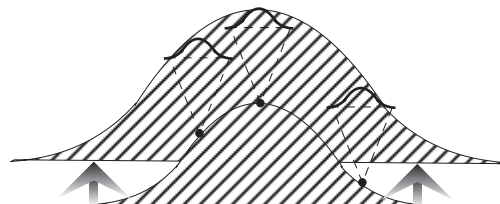


Figure 5.10. The signal created in each point broadens due to the divergent nature of the process.

calculate a spread function that tells how much each point on the original autocorrelation signal will have broadened after a certain distance from the nonlinear medium (Fig. 5.10). A simple convolution between the spread function at this distance and the original autocorrelation signal gives the detected signal. Note that the broadening is calculated only in direction of the delay axis. Figure 5.11.a shows the result of such simulations calculating the size of the signal at a distance of one meter from the nonlinear medium for the interpulse angle $\beta=3.73^\circ$, which is an angle used in the following experiments. The result is indeed stunning. The signal pulse is magnified a great deal with the chosen β angle. If the angle is reduced to $\beta=1.38^\circ$ another angle used in the following experiments, the signal is not broadened at all (Fig. 5.11.b).

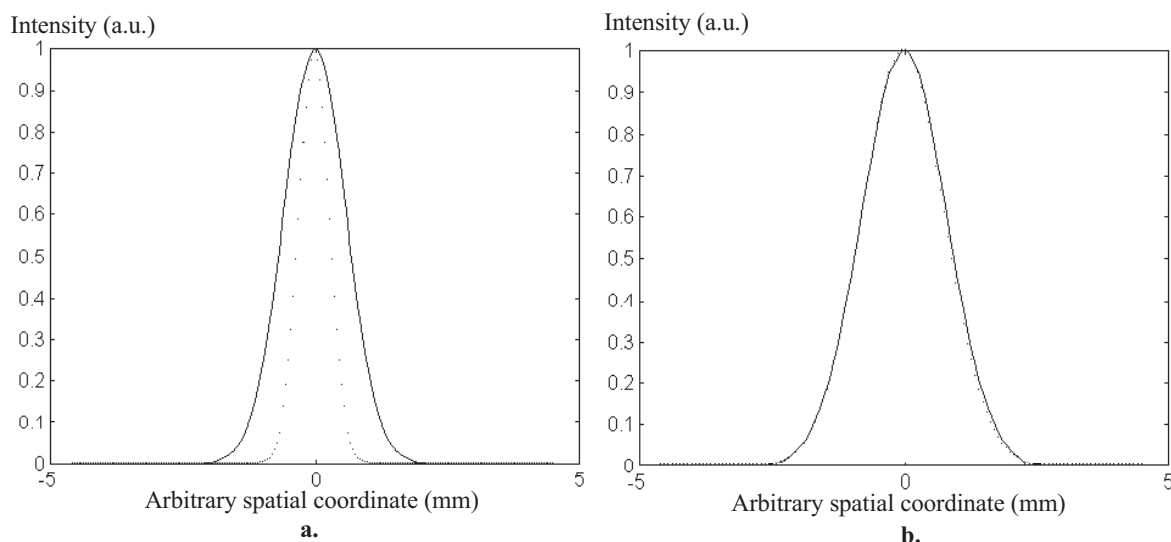


Figure 5.11. The autocorrelation signal broadening after propagating 1 m for different interpulse angles. The original signal is dotted, the broadened is solid. Please note that the lines are almost superimposed in (b). (a) $\beta=3.73^\circ$ and (b) $\beta=1.38^\circ$.

A question needs to be answered still. The conclusion of the simulation seems to be that the shorter the pulse is the more divergent will the signal be. But the condition for this is that the laser pulses are transform limited. As pointed out in Chapter 1.3 the laser pulses always have the same spectrum, even if they have different lengths because of chirp. Consequently, longer pulses should be broadened more than the simulation tells. If the laser pulse is chirped the same simulation as above can be done, but it will be much more difficult. To simplify, the effect is analysed in a worst case simulation. In this, the spectral width is set to correspond to a 110 fs transform limited pulse, even if the actual pulse duration is much longer. Still all frequencies are assumed to be in every point, even though this is not true for chirped, longer pulses. The first simulation serves as a best case. Assuming an ordinary autocorrelator measures the pulse duration at an angle of $\beta=3.73^\circ$, the pulse durations that should be measured using the best and worst case simulations above are calculated. They are plotted together with the actual measured pulse duration in Figure 5.12. The imagined autocorrelator would lead to believe that the pulse duration is somewhere in between the simulation curves. Any such value will be high compared to the actual pulse duration.

The simulations have only calculated the broadening of the signal. But the very nature of the broadening adds another problem. The spectrometer that is used to frequency resolve the signal, sees the signal through a very thin input slit of 120 μm . It is the broadening along this slit that has been calculated. But the signal will be broadened perpendicular to the slit also. Different signal frequencies will travel in different directions, as stated, but this will lead to that some frequencies have a higher probability to pass through the slit than others. Consequently will the spectra that the FROG trace consist of be false. No simulation of this frequency loss is done, but it is important to remember that this problem might affect measurements as well. A solution to the frequency loss is to collect the whole signal in the spectrometer.

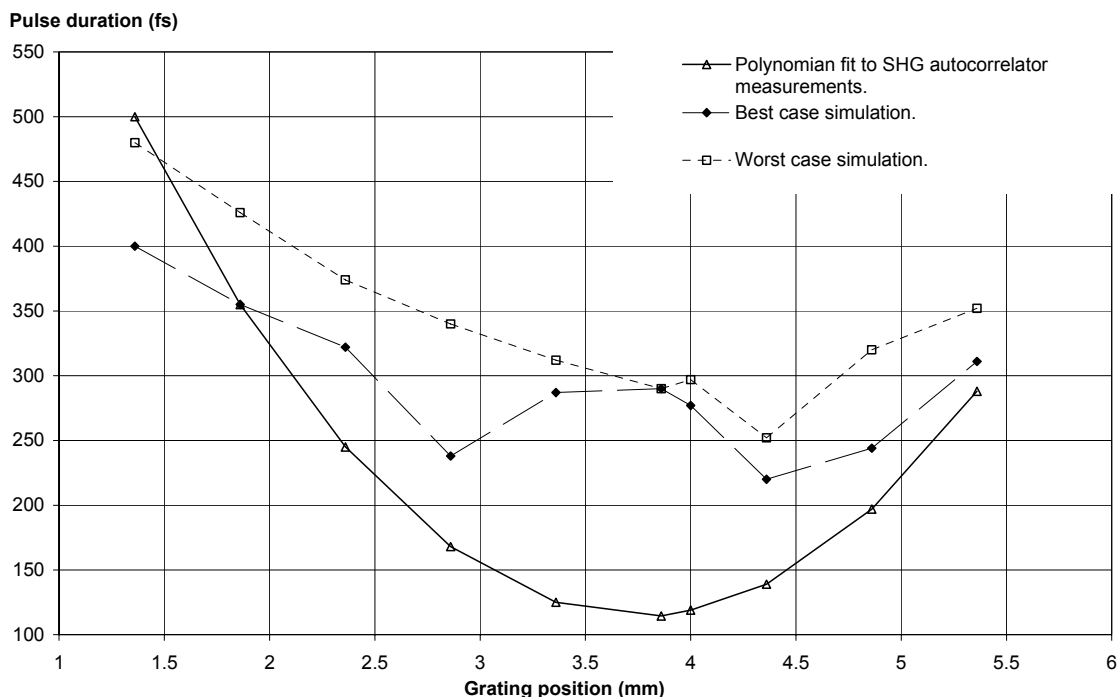


Figure 5.12. The measured pulse durations with an SHG autocorrelator. The worst and best case measured pulse durations for the prototype TG FROG according to simulations.

6 Equipment

6.1 Light splitting and transport

A number of different components are used to split a part of the pulse from the laser laboratory into the laboratory where the FROG stands. The best way to split of a part seems to be with a glass wedge (Fig. 6.1). It reflects only a fraction of the light intensity (about 4%), and no second reflex will follow the main pulse.

When the pulse enters the FROG lab two different setups are used (Fig. 6.2). Sometimes the pulse just passes two mirrors turning the polarization by 90° . This is done because the mirrors in the FROG reflects s-polarized¹⁶ light best. Sometimes the pulse first passes a 5:1 telescope. The telescope increases the pulse intensity by a factor of 25.

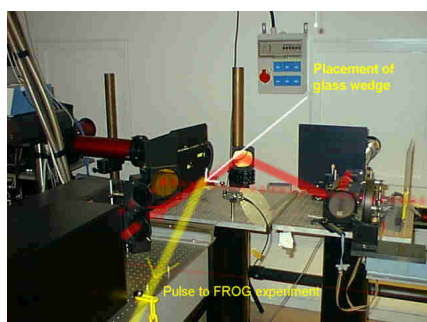


Figure 6.1. The glass wedge splits of about 4% of the pulse as it exits the compressor.

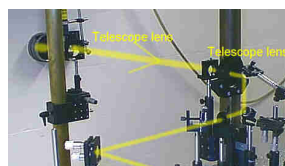


Figure 6.2. The telescope and the two polarization turning mirrors.

6.2 Mirrors, beamsplitters, lenses, filters and optomechanical components

All mirrors used in the FROG are of the same type, namely CAG003 from WELAND technics. They are silver coated, 25 mm diameter, 3 mm thick and reflect more than 95% of s-polarized light.

The TG FROG setup includes two $\lambda/10$ beamsplitters (633 nm) with reflection/transmission of 33%/67% and 50%/50%. EKSMA manufactured them specially for the FROG. They are 25.4 mm in diameter, 1 mm thick, anti reflex coated on one side, made of UV grade fused silica. The angle of incidence (AOI) is 45° and the light should be s-polarized.

The lenses used in the FROG are listed in Table 6.1 together with their primary use. A chromatic¹⁷ cylindrical lens is ordered from EKSMA to be used in the FROG but it was damaged during manufacturing and has not yet been delivered.

Many different filters are used to reduce signal strength or to filter out frequency doubled signals¹⁸. The mirror mounts are as small as the mirrors to allow for small angles in the FROG. The translation stages have a resolution of about $5 \mu\text{m}$. The mounts for the nonlinear medium and the cylindrical lens make it possible to experiment with angles and positions. These mounts are mounted on small translation stages to make sure that the nonlinear medium always can be placed in the lens focus.

¹⁶ If the light is polarized vertical to the plane of incidence it is said to be s-polarized.

¹⁷ To minimize the added chirp.

¹⁸ When aligning the FROG with the help of a KDP crystal.

Table 6.1 List of optics.

Type of lens	Material	Focal length (mm)	Diameter (mm)	Use
<i>Cylinder</i>	<i>Not known</i>	<i>300</i>	<i>51x61</i>	<i>To focus the pulses in the nonlinear medium</i>
<i>Cylinder</i>	<i>Not known</i>	<i>105</i>	<i>50</i>	<i>Focus FROG signal on input slit of spectrometer</i>
<i>Planar-convex</i>	<i>Glass</i>	<i>270</i>	<i>88.9</i>	<i>Multiple shot TG FROG</i>
<i>Planar-convex</i>	<i>Glass</i>	<i>1000</i>	<i>50</i>	<i>5:1 telescope</i>
<i>Planar-concave</i>	<i>Not known</i>	<i>250</i>	<i>25</i>	<i>5:1 telescope</i>

6.3 Nonlinear medium

No special medium is bought for the FROG, but many different crystals and glasses are available at the division. Figure 6.3 is a picture of the different nonlinear medias used.

6.3.1 KDP

The first experimental work is with a second order autocorrelator using a KDP crystal. These experiments gave the idea of using KDP to align the TG FROG. When doing so, the KDP also proves to be a useful nonlinear medium for creation of the FROG signal. However, as made evident in Chapter 7.6, the KDP crystal probably should not be used for TG FROG measurements. The KDP crystal is about 1 mm thick, cut at an angle of 53° to the crystal axis.

6.3.2 SiO₂ - quartz

Two different kinds of quartz were used. A crystalline (α -SiO₂) window, 2.8 mm thick, and an amorphous (non-crystalline fused silica), 0.55 mm thick. Crystalline quartz has a refractive index of $n=1.54$ at 800 nm, neglecting the birefringence. For fused silica it is $n=1.45$.

6.3.3 BK7 glass

To be absolutely sure that the nonlinear medium is amorphous, regular BK7-glass is used as a nonlinear medium. It is 0.6 mm thick and has a refractive index of $n=1.51$ at 800 nm.

6.3.4 Other

There are infinitely many possible media, but one can say that non-crystalline are preferable. Also, the response time of the medium should be short, at least if used in a single shot FROG [18]. A non-crystalline medium can be used with any angle because the refractive index is not a function of the polarization of the light. If the interpulse angles are small in the TG FROG essentially any medium with proper nonlinearity and short response time could be used. Looking in tables one can easily find media that have nonlinearities four orders of magnitude greater than for example SiO₂ [30,45,46]. Unfortunately, these media often have a very long response time.

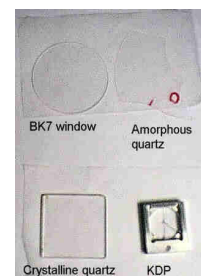


Figure 6.3. The tested nonlinear media.

6.4 Imaging spectrometer

The spectrometer is a crucial part of the FROG setup and it is important to know exactly what it does with the traversing pulse. Spectrometers usually used have a very large astigmatism, which does not affect spectrum recordings, in for example multi shot FROG measurements. The single shot FROG trace, however, is a two dimensional signal, and the spectrometer must not distort the delay axis. Therefore, an imaging spectrometer is an absolute necessity. The spectrometer in the present setup is of model MS 127i™, manufactured by ORIEL instruments. Table 6.2 holds the specifications of the spectrometer, Table 6.3 the grating specifications and Table 6.4 the input slit specifications.

The spatial magnification is an important factor because it affects the delay dispersion of the FROG trace. The worst spatial resolution is awfully high, but is true only for the longest and shortest wavelengths. In the middle of the spectrum the spatial resolution is not specified, but it should be small enough not to affect multichannel measurements since the detector is built for that. The spectrometer is a flat-field imaging spectrometer. It means that one, theoretically, could place a piece of paper a bit from the exit image plane and see a perfect picture of the trace.

Table 7.2. Spectrometer specifications

Input focal length	127 mm
Output focal length	133 mm
F/number	F/3.7
Magnification	
Spectral direction	1.2
Vertical to spectral dir.	1.2
Flat-field dimensions	
Horizontal	25 mm
Vertical	7 mm

Table 6.3. Grating specifications

Grating line density (1/mm)	Blaze wavelength (nm)	Type	Peak efficiency	Primary wavelength region (nm)
1200	750	Ruled grating	80 %	450-1250

Table 6.4. Input slit specifications

Slit width (μm)	Slit height (mm)	Resolution (nm)	Use
50	6	0.6	Wavelength calibration
120	12	1.0	FROG traces

6.5 CCD camera and controller

The CCD camera used to record the FROG traces in the exit plane of the spectrometer is a TE/CCD camera from Princeton Instruments, Inc, see Table 6.5. It holds an X-ray sensitive CCD chip, which is an overkill for FROG purposes, but the camera is used for many other measurements as well. An objective is fitted to the camera to reproduce the flat field image exiting the spectrometer on the CCD chip. When the CCD chip is read off the data is sent to a computer for analysis.

The controller is a ST-130 from Princeton Instruments, Inc. It handles the data transfer to and from the camera and the computer. The analog signals from the camera are converted to digital signals sent to the computer and vice versa.

Table 6.5. CCD chip specifications

Chip	<i>512x512 back illuminated with UV coating</i>
Pixel size	<i>24x24 μm</i>
Temperature range	<i>Down to -70°C with water cooling</i>
Dark charge at -50°C	<i>Typically 3-5 electrons/pixel/second</i>
Spatial resolution	<i>≤ 1.5 pixels at FWHM of spectral line</i>
Geometric distortion	<i>Less than 1 pixel</i>
Spectral range	<i>1600 nm down to below 200 nm</i>
Response linearity	<i>Better than 1% over entire range</i>
Uniformity of response	<i>Typically 5-10%, depending on binning</i>

6.6 Computer and software

A computer with software is used to analyse the CCD pictures. The software is WinSpec, for one dimensional measurements, and WinView, for two dimensional measurements. The software allows binning¹⁹ of the CCD chip and to flip and rotate the read data so that delay and wavelength axes have the right directions. WinSpec also has a wavelength calibration routine using the least square method. Unfortunately, WinView does not have this feature. In WinView it is possible to do some image processing. It is impossible to record and/or show 10 pictures per seconds, which would be necessary to record a trace of every single pulse from the laser system.

A computer program for phase retrieval of FROG traces, FROG 1.5 from Femtosoft Technologies, was aquired. To calculate the actual E-field, phase and spectrum of the pulse, the program needs some additional information to the trace.

1. The delay dispersion, that is, femtoseconds per CCD pixel in delay direction.
2. The wavelength dispersion, that is, nanometers per CCD pixel in spectral direction.
3. The central wavelength in the spectral direction.
4. The type of FROG used to record the trace. PG, SD, SHG and THG FROG traces may be analysed with FROG 1.5. Since TG FROG yields PG or SD traces its traces can also be analyzed with the program.

Number one, two and three is used to put the trace on a time-frequency scale, and number four is essential for convergence of the iterative algorithm [14,34,36].

Apart from the pure iterative calculation, FROG 1.5 offers some image manipulative functions, such as different kinds of noise suppression and rescaling of delay, and a routine to cut out the important part of a FROG trace. The latter is very useful when the actual trace does not cover the whole CCD chip. Before FROG 1.5 starts the retrieval procedure, it puts the trace on a two dimensional time-frequency grid of user defined size and scaling, shaped to be used with the Fast Fourier Transform (FFT) algorithm. A larger grid leads to a better retrieval but every iteration will take longer time.

As the retrieval starts, a number of windows appear (Fig. 6.4). It is up to the user to stop the algorithm when the error is low enough and/or when the target and retrieved traces are visually very alike. It has been shown that the error will decrease with time down to either machine precision, if the trace is perfect and without noise, or to a higher value, depending on the amount and type of noise [34,36]. After a couple of minutes, corresponding to a couple of hundred iterations, the retrieved trace usually is as good as possible.

FROG 1.5 saves all data to disk. The output files are

¹⁹ Read many pixels as one.

1. *frog.dat*, contains a log of all the activity of the program. All input parameters, the FROG error for each iteration, the algorithmic technique and the retrieved pulse duration, spectral width, time-bandwidth products $e t c$.
2. *marg.dat*, contains the delay and frequency marginals for the target and retrieved traces.
3. *a.dat*, contains the target trace after manipulations.
4. *arecon.dat*, contains the retrieved trace.
5. *ek.dat*, contains the complex retrieved electric field, the intensity and the phase with the lowest FROG error. The phase is not the total phase, $\varphi(t) = \varphi_0 + \omega_0 \cdot t + b \cdot t^2 + c \cdot t^3 + d \cdot t^4 + \dots$, but rather $\varphi(t) = \varphi_0 + b \cdot t^2 + c \cdot t^3 + d \cdot t^4 + \dots$. The carrier frequency is always the same, so it is subtracted. This makes it easier to detect chirp. The phase of a FT limited pulse is a straight line.
6. *speck.dat*, contains the complex spectrum of the retrieved field, the spectral intensity and the phase as a function of wavelength.
7. *autok.dat*, the second order intensity autocorrelation of the retrieved field.

Before the traces are exported to the FROG 1.5 program the background noise, which consists of dark currents in the CCD chip, is removed. This is done by resetting all pixels with an intensity less than a certain value to zero. The whole FROG trace then lies in an ocean of zeros, something which the retrieval algorithm more or less requires to function properly.

The FROG traces are recorded using the computer program WinView. The file format that FROG 1.5 requires is not supported by WinView, so a short routine is written in Fortran to convert WinView traces into files readable by FROG 1.5.

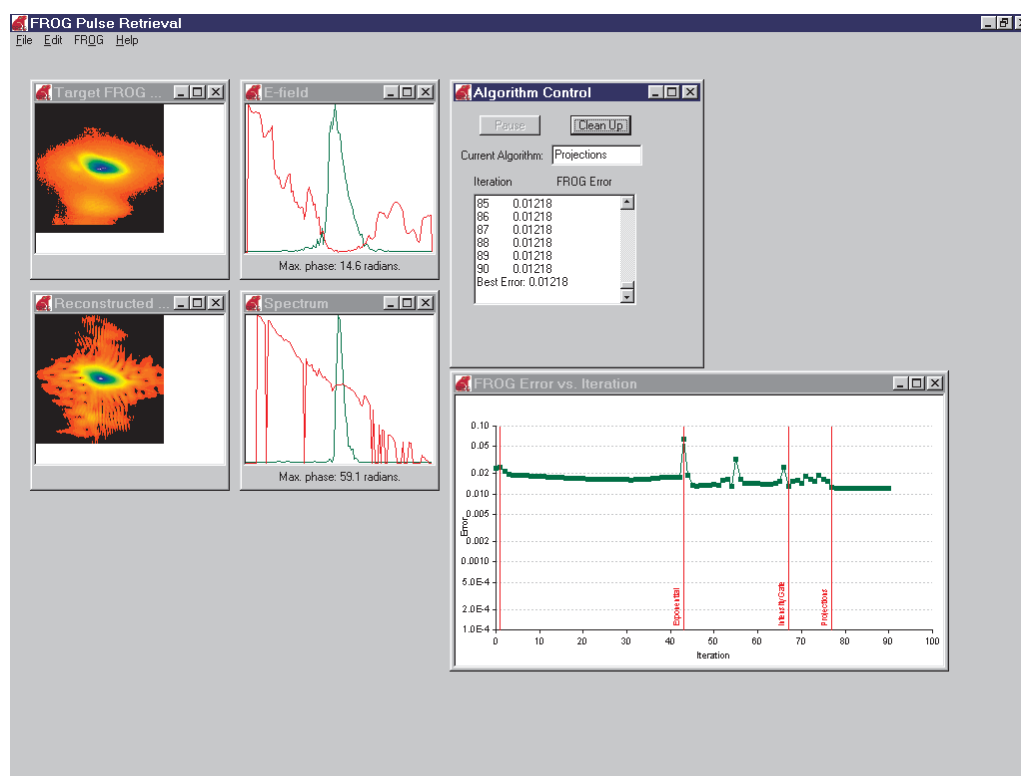
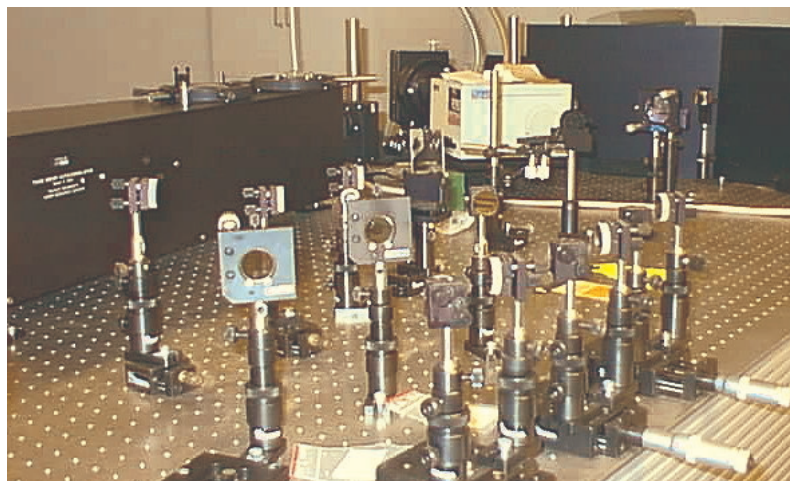


Figure 6.4. FROG 1.5 window as the retrieval algorithm runs. The uppermost windows from the left: The target (measured) FROG trace, the retrieved E-field (green) and phase (red), the control window with algorithm and FROG error. The undermost windows from the left: The retrieved FROG trace, the retrieved spectrum (green) and phase (red), the FROG error graph.

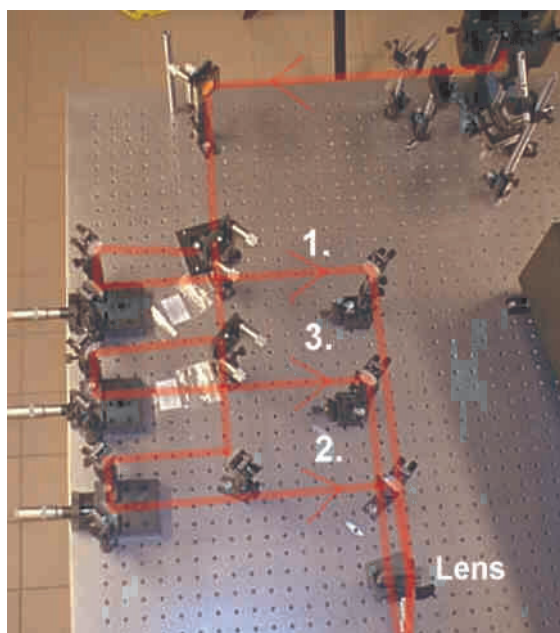
7 Experimental work

7.1 The TG FROG experimental setup

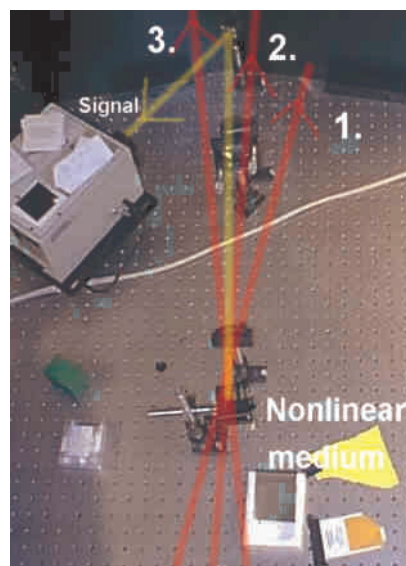
Figure 7.1, 7.2 and 5.6 shows the finished TG FROG setup. The angle, β , determines the delay dispersion. It will be referred to many times in the following sections. The spectrometer and the CCD camera were calibrated before any measurements (App. C and D.).



a.



b.



c.

Figure 7.1. The single shot TG FROG setup. (a) An overview. (b) and (c) The actual setup in comparison with Figure 5.6.



Figure 7.2. An overview of the multi shot TG FROG with spherical lenses pointed out.

7.2 Secure alignment and optimization to get an undoubtable, true TG FROG signal

Experimental work with the SHG autocorrelator gave the idea of using a KDP crystal in the FROG setup to align the pulses. Two pulses overlapping in time and space in a KDP crystal creates three second harmonic pulses (Fig. 7.3).

Two of them are colinear with the pulses and are created even if the pulses do not overlap. The third, however, is created only if the pulses overlap and it has a direction of the bisector of the laser pulses direction [31,32]. Because KDP has a certain response time and the interpulse angle is small, the bisector signal will be an intense line, where the overlap is good, and a weak background of the same size as the pulses. It is therefore easy to align two beams to be at the same place at the same time. Place the KDP crystal in the nonlinear medium holder and place a piece of paper in the path of the pulses after the crystal.

1. Adjust the lens so the focus is in the KDP crystal.
2. Adjust mirrors to make sure the paths of pulse one and two overlap. This is easy.
3. Move the translation stage of one pulse until the bisector second harmonic pulse appears on the paper (Fig. 7.3).
4. Make sure that the crossing occur in the middle of the pulse cross section. It is done by adjusting the delay so that the intense line in the bisector signal precisely cuts the round spot in in the middle.

Now pulse one and two are aligned. Pulse three is aligned in the same way but with more difficulty. If it is in the same place at the same time as the other two pulses all three will interact. Therefore they will create three colinear second harmonic pulses, and three bisector second harmonic pulses (Fig. 7.4).

5. Adjust the mirror of pulse three so that its path visually crosses the path of the other two. This is rather difficult.
6. Move the translation stage of pulse three until six spots appear on the paper. If only five spots appear it is due to that two pulses overlap at two different places in space. For example, pulse one and two overlap at one position and pulse one and three at another, but pulse two and three never overlap. The only way to correct this is to begin again with step five.
7. Make sure the intense lines all cut the signal spots in the middle.

When all seven steps are done the three pulses are in the same place at the same time and they overlap in the middle of their cross sections. Additional interesting processes can occur in the crystal when all three pulses are aligned (App. B). Practically the alignment is a lot more problematic than described above. The KDP crystal only allows second harmonic generation at certain angles because of the phase matching condition [31,32]. Therefore, one has to change the position of the KDP crystal during alignment. This puts the crystal out of focus, so the lens must be adjusted. When the lens is adjusted the pulses aligned in step one to four will not overlap perfectly so step one to four must be redone.



Figure 7.3. Fluorescing paper with three light spots. Note that the bisector SHG signal is a line on a background.

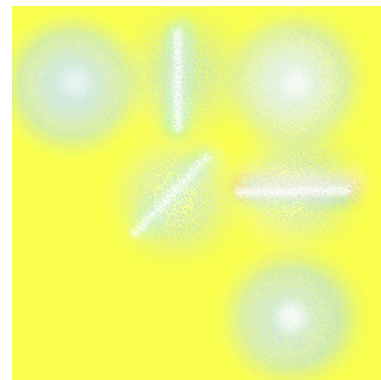


Figure 7.4. Three overlapping beams creating three bisector SHG signals.

And so on... To begin with it took about two hours, but after some practice only about half an hour. Fortunately, if one takes care and makes sure the laser pulses always enter the FROG in the exactly same direction, this difficult alignment only has to be done once.

If all pulses are correctly aligned a TG FROG signal is created. It is normally very weak directly after the alignment with the KDP crystal, however. The third order process creating the FROG signal is much more sensitive to non perfect alignment than the second harmonic process used to align the pulses. Therefore one has to optimize the FROG signal after the first alignment. This is done by

1. changing the distance between the lens and the nonlinear medium to center the focus in the medium,
2. adjusting the mirrors and the translators to find the maximum intensity of the signal so that all three pulses overlap as well as possible.

This optimization procedure is also difficult, because the mirror mounts are put on long rods and because of the limited resolution of the mirror screws. If a finger barely touches a mirror mount, the signal may disappear completely. One must therefore use extreme care adjusting the mirrors. Had the mounts been more stable this problem would have been reduced. However, more stable mounts would have lessened the mount flexibility. When buying the equipment flexibility was chosen. In a final, more permanent setup, stability should be given priority.

7.3 The IR sensitive camera

Since the FROG signal is so weak that it is practically invisible, it is impossible to direct it into the spectrometer by direct vision. The signal and laser wavelength is 800 nm, where the eyes are extremely insensitive. Even with the small IR viewers often used to see the laser light, one can not see it. Another type of IR sensitive camera, connected to a monitor, is therefore used to view the input slit of the spectrometer. As soon as the signal is directed close to the input slit, the fine tuning of the direction can be made with help of the camera and monitor.

7.4 Alignment from day to day

When the first alignment was done, several apertures were put in the laser pulse path, and a part of the pulse was reflected with a piece of glass onto the wall, where a marking was drawn. Together, the apertures and the marking define an optical axis along which the pulse always should travel. Every time the laser is shut down, the pulse can be directed through these apertures and onto the marking. If this is properly done the pulse travels along the exactly same path as the other day, and therefore no new alignment has to be done in the FROG. At first, the FROG signal seemed so sensitive to changes in direction that it seemed inadequate with this day to day alignment. Therefore it was surprising to get a strong FROG signal every time the laser pulse path was aligned to the optical axis. This implies that a TG FROG easily can be used as a monitoring equipment in a laser lab, without the need of everyday alignment. To maintain a strong signal from day to day, however, the best solution is an automatically beam aligning system. It could be realized for example with three photo diodes acting as input to a regulator that can change the position of the two first mirrors in the FROG setup. If the regulator always maximizes the photo diode signals a continuous alignment can be achieved.

7.5 Stray light

Although the TG FROG gives theoretically background free signals, the situation is in reality a bit more complicated. Of the nonlinear media, KDP gives most stray light by far even though it is not the thickest. It is probably because the KDP allows so many different nonlinear processes (Table B.1). Specifically a 2ω pulse has the same direction as the FROG signal. Even though a filter is used to block any 2ω radiation it may be intense enough to give a background to the FROG signal. In general the stray light increases, as does the signal intensity, with material thickness. The stray light is also a function of the spatial and time overlap of the pulses. The better overlap the more stray light, unfortunately.

7.6 KDP - no good for FROG traces

As mentioned, the KDP crystal gives a lot of stray light. This is not the only problem. In some way, which is not fully understood, the KDP creates an additional well defined signal that has the same direction as the FROG signal. It is not the 2ω radiation already discussed. When the delay of pulse one is changed, the FROG signal travels in the vertical direction as it should²⁰. But the additional signal does not move at all. It appears to be much less sensitive to pulse overlap than the true FROG signal. This would be true of a second order process, but a second order signal could not be phase matched in that direction. It could be that a grating is built up that is almost permanent or some kind of surface nonlinear process like for STHG FROG, but both are very unlikely. The fact that many different nonlinear processes take place in the KDP crystal speaks against it also. If a lot of energy is used for other processes the FROG signal will be weakened. Perhaps some processes take away frequency components from the pulses. In such case the FROG trace will not be useful. The conclusion is that a KDP crystal should not be used to do TG FROG measurements. It is still very useful for alignment purposes, though.

7.7 TG FROG traces without the cylindrical lens

The cylindrical lens is used to increase the intensity in the interaction region to produce a stronger signal. If the lens is removed, however, much can be won.

1. The pulses will not gain additional chirp passing through the glass.
2. Alignment is likely to be easier.
3. If the pulse is spatially sheared, focusing leads to useless FROG traces.

To see if it is possible to omit the lens it was taken away and the setup readjusted. In order to have sufficient intensity, a telescope was built before the FROG to reduce the size of the laser pulse down to one fifth of its original diameter, leading to twenty five times higher pulse intensity. The first alignment is tedious because of the low power in the interaction region which makes it difficult to see even the non colinear SHG beams. A window of BK7 glass was used as nonlinear medium. Measurements with this setup is presented in Chapter 8.1.

Although the first alignment is much more difficult without the lens it should be easier in the long run. The reason is that it is easier to see to that all three the pulses overlap in step four of the alignment procedure.

²⁰ This is not obvious until one studies figure 5.7 and figures out how the interaction region will move as pulse one is delayed.

7.8 Multiple shot TG FROG

To verify the results obtained in the single shot setup, the FROG was rebuilt to give multiple shot traces. In short, the cylindrical lens was replaced by a spherical lens so that the three pulses overlap in one very small point only. A second lens focused the signal into the input slit of the spectrometer. The translation stage of pulse one was scanned and for every 5 μm a spectrum of the FROG signal was recorded. The signal intensity fluctuated rather much, so each spectrum is a sum of 50 FROG signal spectra. Together, the spectra form a multishot FROG trace (Ch. 8.2).

7.9 Changing the distance between the compression gratings

The CPA system in Lund uses gratings to expand and compress the laser pulse. When the compressor grating distance is changed, the amplified, positively chirped, pulse is compressed more or less efficiently. The greater the distance, the more efficient is the compression. But, if the distance is too large, the compressor will not only remove the positive chirp, it will give the pulse a negative chirp. It will then enter the compressor with a positive chirp and exit with a negative chirp. There exist a position where the pulse is optimally compressed. On this laser system it is known to be when the grating translator reads about 3.8. The chirp created in a CPA system elongates the pulse in time, but does not change its spectrum. FROG traces are recorded at different grating positions. It should be possible to determine the corresponding pulse chirps and lengths by looking at the trace and/or using the retrieval algorithm and to find the optimum grating position (Ch. 8.1). Perhaps will such measurements verify the position for ideal compression. In Appendix G, the acquired linear chirp due to propagation is calculated. The CPA system does not only give the pulse linear chirp, but also higher orders of chirps. Travelling from the laser to the FROG the pulse acquires linear chirp because of Group Velocity Dispersion (GVD) and Self Phase Modulation (SPM) (App. G). The pulse also passes through two beamsplitters and one, two or three thin lenses on its way to the nonlinear medium. Because of GVD and SPM in these, the pulse acquires more positive linear chirp. SPM gives the pulse higher orders of chirp also, but mainly linear chirp. When using the 5:1 telescope, the intensity of the pulse increases 25 times, leading to even more SPM. In total, the pulse will acquire roughly $+190 \cdot 10^{24} \text{ s}^{-2}$ of linear chirp. An increased grating distance would beforehand compensate for the linear chirp acquired by travelling. Unfortunately, such a change in grating distance give the pulse higher orders of negative chirp when it passes the compressor. Consequently, the pulse will not become as short as it could. Even if the negative linear chirp is removed by GVD and SPM, higher orders of chirp remain and prolongate the pulse. The FROG should be able to tell whether this reasoning is true or not.

8 Results from experimental measurements

As the FROG traces are recorded they have to be analysed. Looking at the trace, it is possible to say some things about the pulse, but it is necessary to use the phase retrieval algorithm to know exactly what the pulse looks like, both in time and frequency (Ch. 4.2). For this reason the computer program FROG 1.5 from Femtosoft Technologies is used. Interesting results and conditions are given in Table 8.1 below. (The FROG traces are referred to by their figure numbers, leaving out the chapter number.)

8.1 Single shot TG FROG

A number of different angles, β , were used in the setup (Fig. 5.6). To begin with, the angle was $\beta=0.93^\circ$ in the KDP crystal. Traces recorded using this angle turned out to be too large for the spectrometer to handle, so the angle was increased to $\beta=1.38^\circ$. An example of the traces recorded at this angle is depicted in Figure 8.1. It is a bit noisy, but after some image processing, the retrieval algorithm is able to converge reasonably well. In fact, the algorithm is run on most traces taken at this occasion, but the results are the same (Table 8.1).

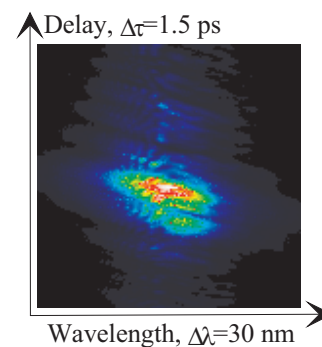


Figure 8.1. FROG trace when $\beta=1.38^\circ$ and the grating translator reads 2.86 mm.

To reduce the trace size even more, the angle is increased to $\beta=3.73$. Looking at Figure 8.1, this might seem unnecessary. It is, however, important to be able to remove noise with apertures and such, and increasing the angle makes it easier to see noise in the trace. A selection of measurements with this angle is held in Table 8.1. Figure 8.2 and 8.3 shows traces recorded at this angle. If the FROG trace intensity histogram is manipulated, one can make the lower intensity structures visible (Fig. 8.4).

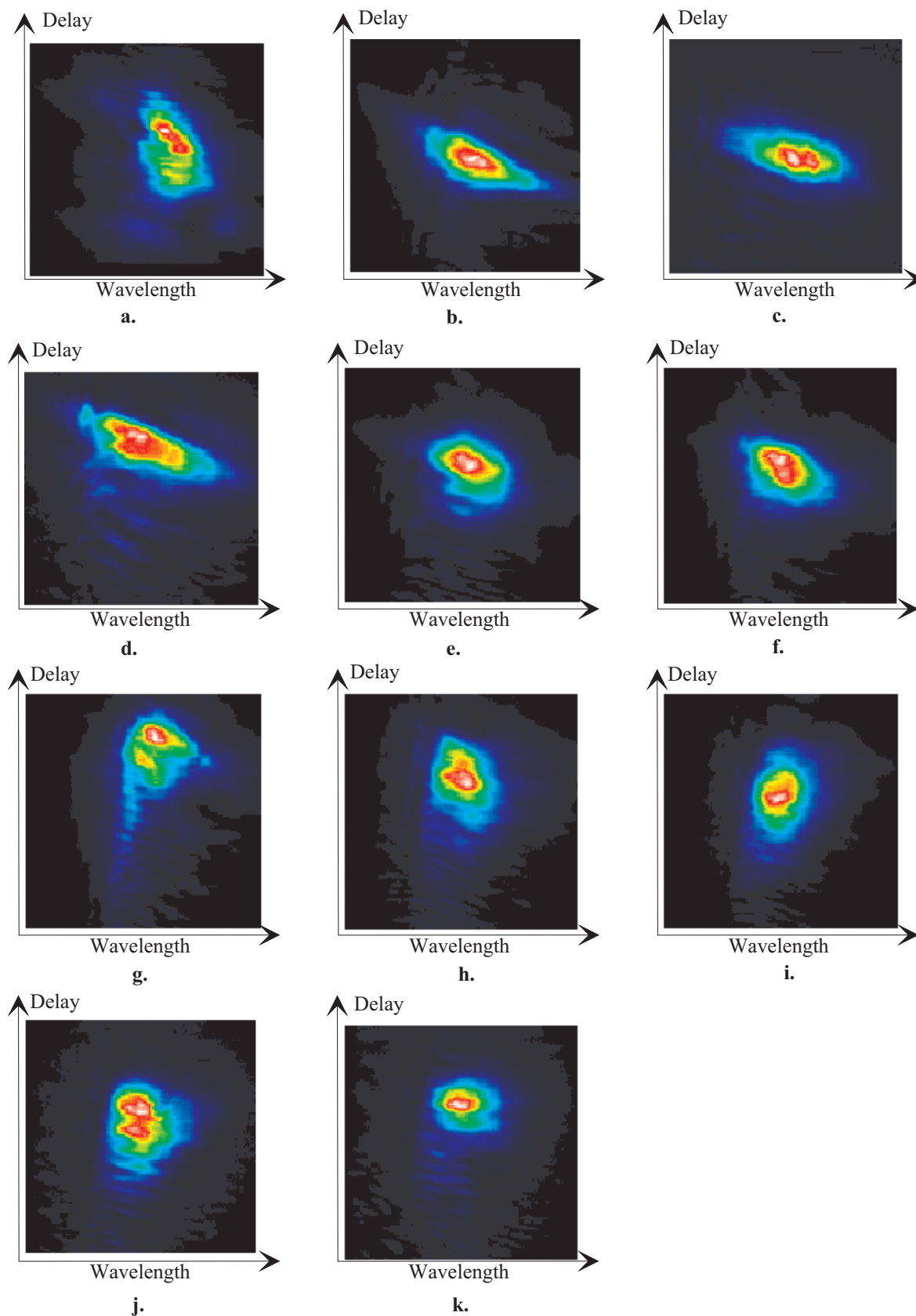


Figure 8.2. FROG traces recorded with fused silica as nonlinear medium. The grating translator reading (mm) was (a) 2.0 (b) 2.7 (c) 3.4 (d) 3.9 (e) 4.4 (f) 4.9 (g) 5.4 (h) 5.9 (i) 6.4 (j) 6.9 (k) 7.4.

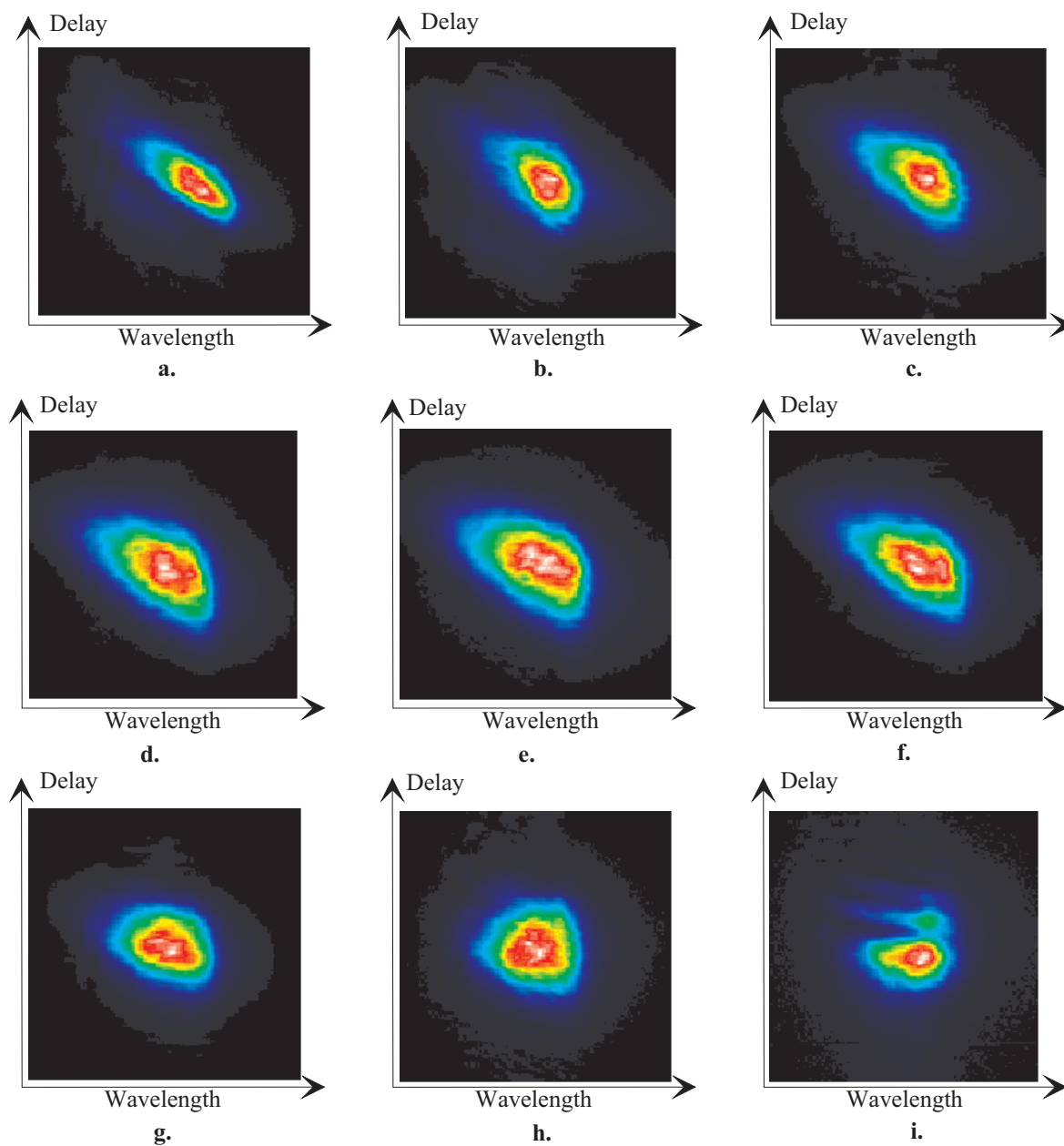


Figure 8.3. FROG traces recorded with BK7 as nonlinear medium. The grating translator reading (mm) was (a) 1.36 (b) 1.86 (c) 2.36 (d) 2.86 (e) 3.36 (f) 3.86 (g) 4.36 (h) 4.86 (i) 5.36.

With the present equipment the dynamic range is about 14 bits, so even very low intensity structures can be made visible. The odd small structures lie far from the central wavelength, but are not noise. They appear in every trace FROG trace from the T³-laser.

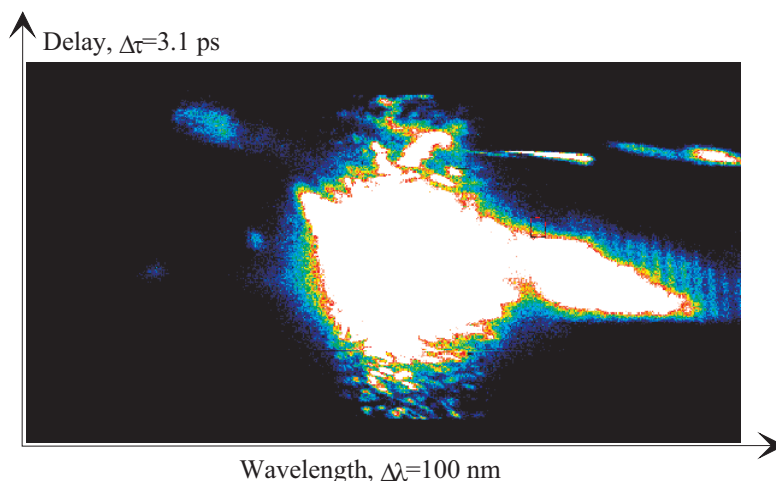


Figure 8.4. A FROG trace (2.b) with visible low intensity structures.

Trace 1 gives an almost perfectly retrieved pulse duration, according to SHG measurements (Table 8.1). The trace is recorded using an imaging lens. Otherwise, the retrieved pulse duration is constantly too long. Some exceptions can be found when the grating displacement is the largest. In addition, the retrieved pulses do not have wide enough spectra. Remember that a pulse of a certain length must, at least, have a correspondingly wide spectrum. Even if the pulse is not ideally compressed, it will contain all frequency components needed for a 110 fs pulse, so the spectrum width should be about 8.5 nm. For the retrieved fields this necessary condition is not satisfied, which leads one to believe that the results are no good at all. However, it will be made plausible that these impossible results are in fact the result of a certain physical effect.

Looking at the traces in figure 8.2 and 8.3, the ones taken at grating translator readings of between 4.36 mm and 5.36 mm, look different. Recalling the discussions on the general FROG trace the looks of these traces imply that the laser pulse has little chirp. But according to measurements the ideal translator reading is about 3.8 mm. At least if the pulse duration is important. As discussed in Chapter 8.9, the laser pulse gains chirp when it travels. In theory, the linear chirp of the pulse is minimized when the grating distance is larger than the ideal distance. How much larger depends on the compressor characteristics and on the exact laser pulse path. Trace 2.g, taken at a translator position of 5.4, and 3.i, taken at 4.86, indicate about zero chirp. The retrieved intensity and phase for Trace 2.b is given in Figure 8.5. Clearly, the characteristic parabolic phase indicates positive chirp. Figure 8.6, which is the retrieved intensity and phase of Trace 2.g, indicate very little chirp. Apparently is a visual examination of the traces enough to determine if the pulse has a chirp or not. The reason that the zero chirp position is different for Trace 2.g and 3.i, 5.4 and 4.86 respectively, could be that no focusing lens is used in the second measurement. Propagating through the lens and focused into the medium the pulses acquire twice the chirp that they do if no lens is present (App. G).

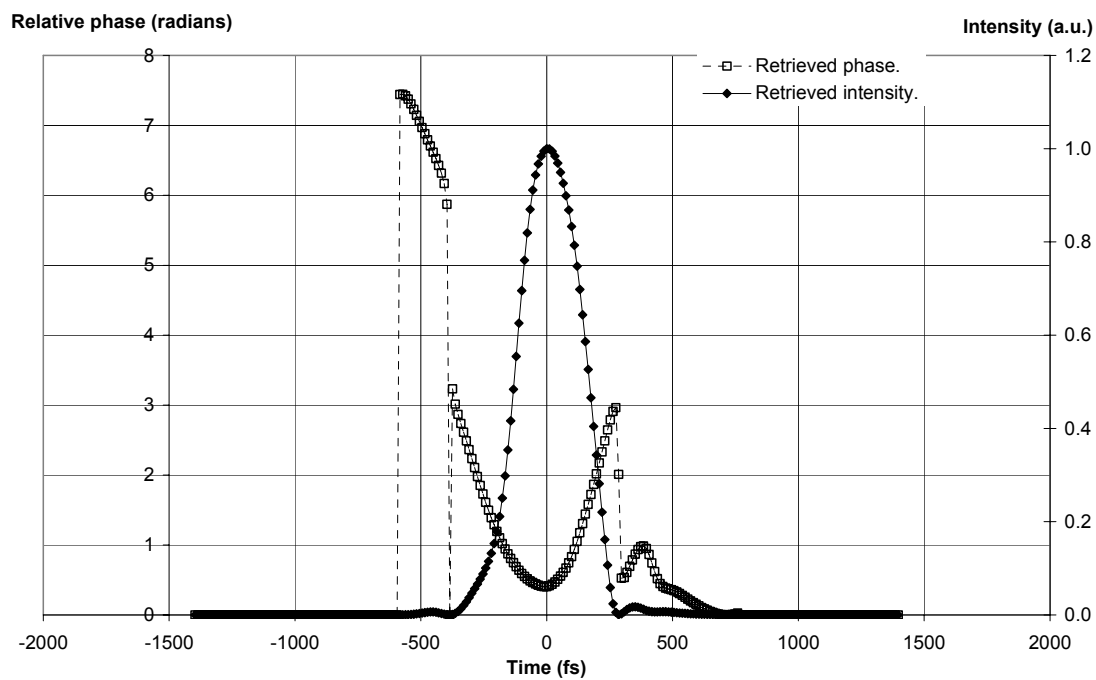


Figure 8.5. The retrieved intensity and phase of Trace 2.b.

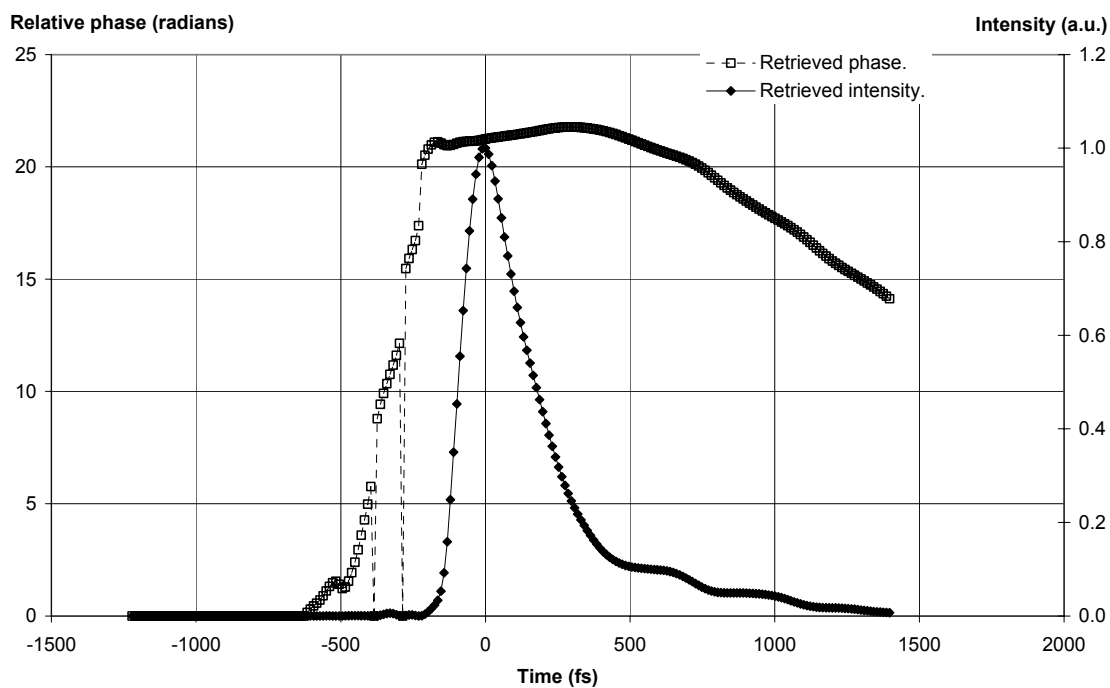


Figure 8.6. The retrieved intensity and phase of Trace 2.g.

The recorded TG traces do indicate the chirp but the retrieval algorithm fails in retrieving useful pulse durations and spectral widths. The errors are most likely not due to the algorithm, but to the traces it works with. There exist a physical phenomenon, innate in all optically nonlinear processes, which might lead to a divergent signal. It is partly studied in Chapter 5.3.8 with a simulation. The conclusion of this simulation is that for large enough interpulse angles, the signal will be considerably divergent. The fact that signal frequencies may be lost because of this effect is also discussed. Figure 8.7 shows the pulse durations as predicted by the simulations, measured with an SHG autocorrelator, and as retrieved from the FROG traces in Figure 8.4. The pulse durations retrieved and those calculated in the simulations agree well. This indicates that the “only” problem with the FROG traces is that the autocorrelation has been done at a too large angle, β . This would also explain why the spectra of the retrieved pulses are so narrow (Ch. 5.3.8). The fact that the correct pulse duration is retrieved from Trace 1 is also in agreement with the simulations. The angle used for that trace, $\beta=1.38^\circ$, is so small that the divergence should be negligible according to the simulations. Still, something speaks against that the only explanation is divergence. The spectral width of the retrieved pulse is too narrow for Trace 1. It is only 6.4 nm , but it should be about 8.5 nm if the shortest pulse is assumed to be 110 fs . This might be because the trace is noisy and difficult for the retrieval algorithm, or because the nonlinear medium is KDP. Because of all other nonlinear processes, the pulses might lose frequencies, which in turn leads to a FROG signal with too few frequencies.

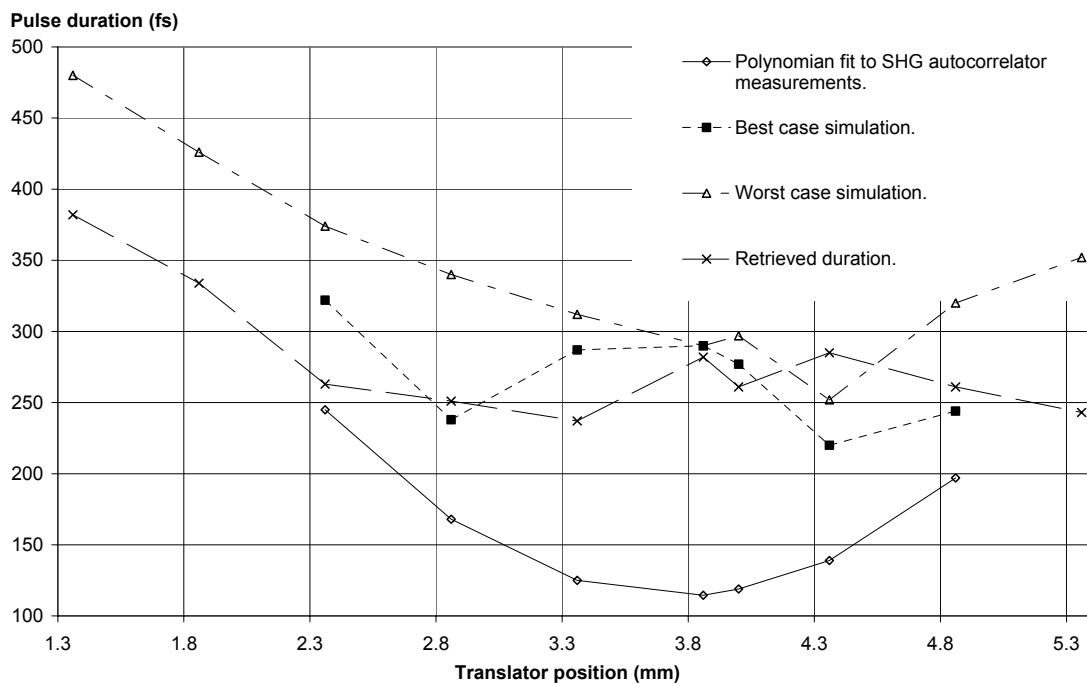


Figure 8.7. Retrieved, measured and simulated pulse durations.

Looking at Table 8.1, another important fact should be pointed out. Almost constantly the retrieved spectral width is narrower for traces taken with the focusing cylindrical lens and without the imaging lens. Traces recorded without the lenses are a bit closer to the truth. Once again this is explained by the divergent nature of the signal. When the cylindrical lens is used, the signal is divergent mainly because the lens has focused the laser pulses, and not because of the divergent nature of the process. The signal has diverged to a width of a couple of centimeters perpendicular to the input slit when it reaches the spectrometer. If frequency loss is a problem, which is likely, then the loss will be severe for such a wide signal. No cylindrical optics means that the signal will be small perpendicular to the slit and that the only diverging process is the one intrinsic in the shaping of the signal.

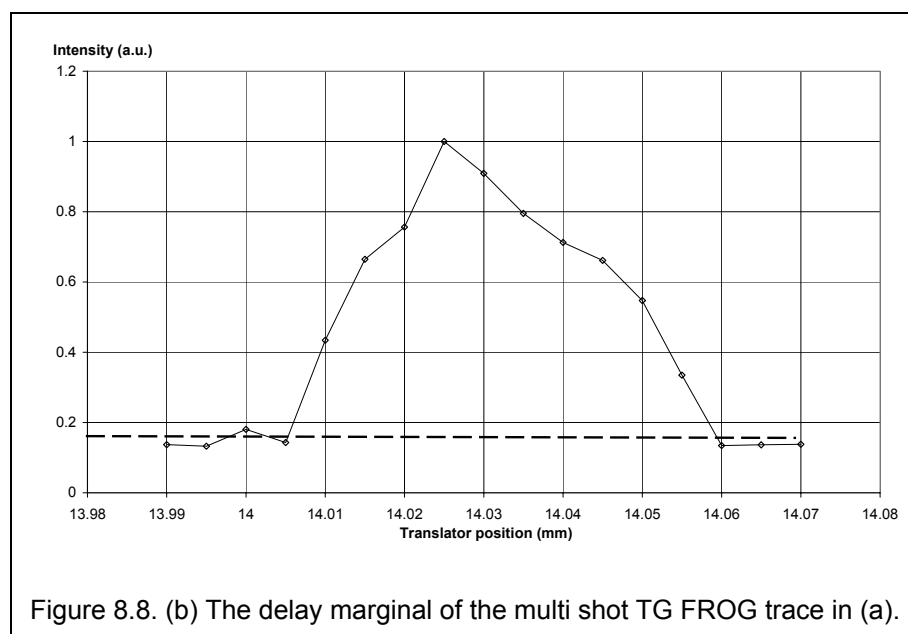
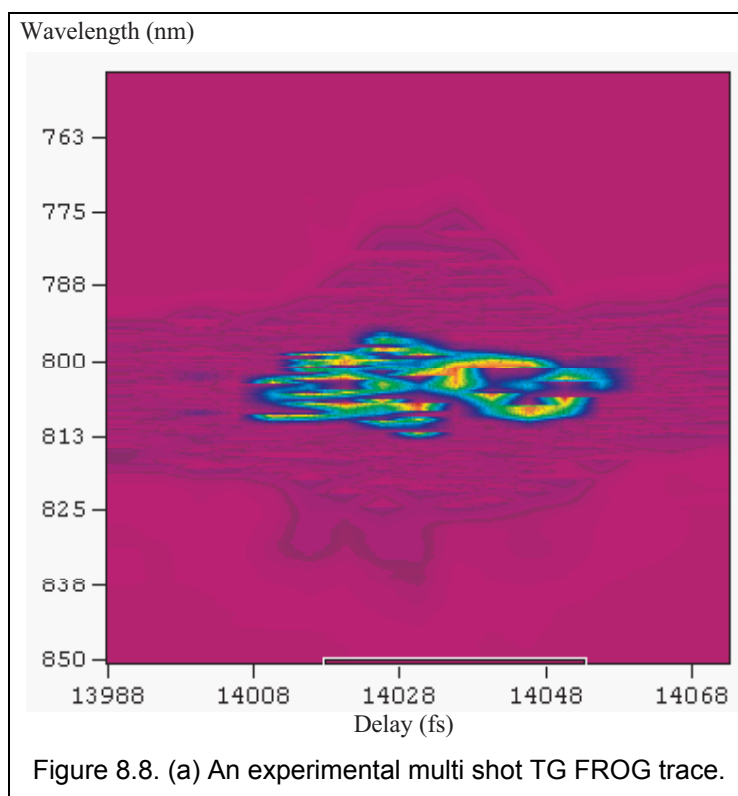
Table 8.1. Summarizing table of interesting experimental conditions and results.

Trace no.	Date	Nonlinear medium	β angle in medium	Telescope	Grating position	Focusing cylindrical lens	Imaging lens	Total pulse energy (mJ)	“Should be” pulse duration ²¹	Retrieved pulse duration (fs)	Spectral width (nm)	Sign of chirp
<i>1</i>	<i>21/10</i>	<i>KDP</i>	<i>1.39</i>	<i>no</i>	<i>2.86</i>	<i>yes</i>	<i>yes</i>	<i>-</i>	<i>168</i>	<i>161</i>	<i>6.4</i>	<i>+</i>
<i>3.a</i>	<i>10/12</i>	<i>Fused silica</i>	<i>3.73</i>	<i>yes</i>	<i>2.0</i>	<i>yes</i>	<i>no</i>	<i>1.6</i>	<i>321</i>	<i>307</i>	<i>2.4</i>	<i>+</i>
<i>3.b</i>	<i>10/12</i>	<i>Fused silica</i>	<i>3.73</i>	<i>yes</i>	<i>2.7</i>	<i>yes</i>	<i>no</i>	<i>1.6</i>	<i>189</i>	<i>299</i>	<i>3.7</i>	<i>+</i>
<i>3.c</i>	<i>10/12</i>	<i>Fused silica</i>	<i>3.73</i>	<i>yes</i>	<i>3.4</i>	<i>yes</i>	<i>no</i>	<i>1.6</i>	<i>123</i>	<i>254</i>	<i>6.6</i>	<i>+</i>
<i>3.d</i>	<i>10/12</i>	<i>Fused silica</i>	<i>3.73</i>	<i>yes</i>	<i>3.9</i>	<i>yes</i>	<i>no</i>	<i>1.6</i>	<i>116</i>	<i>283</i>	<i>6.2</i>	<i>+</i>
<i>3.e</i>	<i>10/12</i>	<i>Fused silica</i>	<i>3.73</i>	<i>yes</i>	<i>4.4</i>	<i>yes</i>	<i>no</i>	<i>1.6</i>	<i>143</i>	<i>286</i>	<i>3.3</i>	<i>+ small</i>
<i>3.f</i>	<i>10/12</i>	<i>Fused silica</i>	<i>3.73</i>	<i>yes</i>	<i>4.9</i>	<i>yes</i>	<i>no</i>	<i>1.6</i>	<i>203</i>	<i>317</i>	<i>2.9</i>	<i>+ small</i>
<i>3.g</i>	<i>10/12</i>	<i>Fused silica</i>	<i>3.73</i>	<i>yes</i>	<i>5.4</i>	<i>yes</i>	<i>no</i>	<i>1.6</i>	<i>296</i>	<i>265</i>	<i>3.23</i>	<i>≈ 0</i>
<i>3.h</i>	<i>10/12</i>	<i>Fused silica</i>	<i>3.73</i>	<i>yes</i>	<i>5.9</i>	<i>yes</i>	<i>no</i>	<i>1.6</i>	<i>-²²</i>	<i>329</i>	<i>2.9</i>	<i>- small</i>
<i>3.i</i>	<i>10/12</i>	<i>Fused silica</i>	<i>3.73</i>	<i>yes</i>	<i>6.4</i>	<i>yes</i>	<i>no</i>	<i>1.6</i>	<i>-</i>	<i>347</i>	<i>3.0</i>	<i>-</i>
<i>3.j</i>	<i>10/12</i>	<i>Fused silica</i>	<i>3.73</i>	<i>yes</i>	<i>6.9</i>	<i>yes</i>	<i>no</i>	<i>1.6</i>	<i>-</i>	<i>337</i>	<i>2.7</i>	<i>-</i>
<i>3.k</i>	<i>10/12</i>	<i>Fused silica</i>	<i>3.73</i>	<i>yes</i>	<i>7.4</i>	<i>yes</i>	<i>no</i>	<i>1.6</i>	<i>-</i>	<i>285</i>	<i>2.4</i>	<i>-</i>
<i>4.a</i>	<i>14/12</i>	<i>BK7</i>	<i>3.73</i>	<i>yes</i>	<i>1.36</i>	<i>no</i>	<i>no</i>	<i>1.6</i>	<i>-</i>	<i>382</i>	<i>4.2</i>	<i>+ large</i>
<i>4.b</i>	<i>14/12</i>	<i>BK7</i>	<i>3.73</i>	<i>yes</i>	<i>1.86</i>	<i>no</i>	<i>no</i>	<i>1.6</i>	<i>355</i>	<i>334</i>	<i>3.2</i>	<i>+ large</i>
<i>4.c</i>	<i>14/12</i>	<i>BK7</i>	<i>3.73</i>	<i>yes</i>	<i>2.36</i>	<i>no</i>	<i>no</i>	<i>1.6</i>	<i>245</i>	<i>263</i>	<i>3.62</i>	<i>+</i>
<i>4.d</i>	<i>14/12</i>	<i>BK7</i>	<i>3.73</i>	<i>yes</i>	<i>2.86</i>	<i>no</i>	<i>no</i>	<i>1.6</i>	<i>168</i>	<i>251</i>	<i>4.3</i>	<i>+</i>
<i>4.e</i>	<i>14/12</i>	<i>BK7</i>	<i>3.73</i>	<i>yes</i>	<i>3.36</i>	<i>no</i>	<i>no</i>	<i>1.6</i>	<i>125</i>	<i>237</i>	<i>4.7</i>	<i>+</i>
<i>4.f</i>	<i>14/12</i>	<i>BK7</i>	<i>3.73</i>	<i>yes</i>	<i>3.86</i>	<i>no</i>	<i>no</i>	<i>1.6</i>	<i>115</i>	<i>282</i>	<i>6.2</i>	<i>+</i>
<i>4.g</i>	<i>14/12</i>	<i>BK7</i>	<i>3.73</i>	<i>yes</i>	<i>4.36</i>	<i>no</i>	<i>no</i>	<i>1.6</i>	<i>139</i>	<i>285</i>	<i>4.7</i>	<i>+ small</i>
<i>4.h</i>	<i>14/12</i>	<i>BK7</i>	<i>3.73</i>	<i>yes</i>	<i>4.86</i>	<i>no</i>	<i>no</i>	<i>1.6</i>	<i>197</i>	<i>261</i>	<i>4.5</i>	<i>≈ 0</i>
<i>4.i</i>	<i>14/12</i>	<i>BK7</i>	<i>3.73</i>	<i>yes</i>	<i>5.36</i>	<i>no</i>	<i>no</i>	<i>1.6</i>	<i>-</i>	<i>243</i>	<i>2.1</i>	<i>- small</i>

²¹ Values from a polynomial fit to measured with an SHG autocorrelator (Ch. 2).²² Outside the interval for the measurements.

8.2 Multiple shot TG FROG

The single shot TG FROG built in this project is easily converted into a multi shot type. The actual measurements are then not as accurate as one can wish because of the low delay resolution of the translation stages. In addition, the FROG signal fluctuates much due to the fluctuating laser pulses, so the errors are large. However, the results are quantitatively better than the single shot results (Fig. 8.8). The FROG trace consists of many spectra taken at different delays, and is interpolated to look nicer (Fig. 8.8.a). The delay marginal of the trace is given in Figure 8.8.b. It has much too low delay resolution to be inverted with the retrieval algorithm, but the approximate pulse duration, $\tau_{\text{FWHM}} = 170$ fs, can be calculated through the delay marginal. The grating position was 4.36 when the trace was recorded. Notice that it looks less smeared in delay. That is another fact which supports the discussion on the single shot TG FROG.



8.3 Conclusion - The Future FROG

An important part of the diploma work is to guide the design of the final FROG that will be a part of the T³-system in Lund. Theory and experiments make it possible to answer a number of interesting questions regarding the future FROG and the actual possibilities of it.

8.4 Difficulties

Higher orders of chirp are difficult to identify by visual examination of the recorded traces. It is a well known and intuitive fact that FROGs in general are less sensitive to higher orders of chirp [19]. CPA systems can give the pulse many high orders of chirp so it is important that the FROG can detect them. There is one way to increase the sensitivity of the prototype TG FROG, however. The angle, β , should be reduced. That will result in larger traces with higher resolution. In such traces higher orders of chirp are easier to recognize. Generally, the minimal angle is limited by the size of input/output of the spectrometer and the size of the CCD chip, so the problem must be thought of before the FROG is built. A second possibility is available if a fast computer can analyse recorded traces continuously. Then the retrieval algorithm, which better regards higher orders of chirp, will retrieve phases that indicates the higher orders.

So far the only results from the FROG are qualitative. A future FROG should be able to give quantitative answers like the amount of chirp, including higher orders, and the exact pulse duration.

The equipment used in the prototype FROG is very flexible, at the cost of stability. Any measurement requires stability for accurate results. A future FROG do not need the flexibility of a prototype.

Because the CCD chip is a square, but the image plane of the spectrometer is a rectangle, only a part of the CCD chip is used for trace recordings. In addition, it is very important to fix the camera and spectrometer relative to each other. Every time the camera or spectrometer is moved, delay- and wavelength calibrations must be redone. The objective that images the spectrometer output on the CCD chip is an unnecessary part of the setup, adding to the uncertainties. A camera with a CCD chip which can be mounted directly in the output plane of the the spectrometer would be preferable.

Another very important improvement is to move the FROG. The prototype stands in a laboratory about ten meters from the laser. On the way to the FROG several physical processes may change the pulse. If the FROG is to be used to optimize laser performance, it must stand close to where the amplified, compressed laser pulse leaves the laser. If the laser is optimized to give a perfect trace without chirp in the FROG several meters away, the laser will not run optimally, as one might be led to believe. If the FROG is built to be easily transported from one laboratory to another, it can be used to characterize the laser pulse in a particular experimental setup. This could be most helpful, because some experiments are very sensitive to any type of chirp, including any aquired in the pulse transport from the laser to the experiment.

Online measurements are not possible with the present setup because the camera/controller/computer part is too slow.

The present FROG setup is not suited to measure laser pulse shearness. When a cylindrical lens is used, any shearness in the direction of focusing will be detected because the trace will become longer in time. Unfortunately, it is not possible to obtain a clear picture of the shearness with this information only. Other techniques allow much better characterization of pulse-front distortions [47].

8.5 Solutions

To achieve quantitative results everything points in the same direction. Reduce the angle β as much as possible without collecting too much stray light and use only amorphous nonlinear media, such as BK7. If a cylindrical lens is used, a second imaging lens must be used so that the whole signal is collected in the spectrometer, otherwise frequency components are lost.

If the optomechanical equipment is optimized for a future FROG with fixed parameters, the experimental difficulties will be reduced and the setup will become much smaller.

The CCD camera should be fastened to the spectrometer at the output and the size of the CCD chip should match the size of the output image plane. In such case, alignment has to be done only once, even if the spectrometer/camera part is moved.

Depending on what the FROG will be used for, optimizing laser performance or measuring the actual pulse shape and phase in an experimental setup, different conditions apply. The first situation demands that the FROG is placed close to the laser, but the latter demand that the FROG is portable so it can be transported from one experiment to another. No matter what the use might be Transient Grating is the recommendable type of FROG. The lack of phase matching conditions and the good sensitivity clearly outmatches the practical problem of aligning three pulses. Only PG FROG have the same advantages but it is not background free, which is a severe drawback, and requires high quality polarizers.

The recording part of the present FROG prototype lacks one quality if it is to be used in an online FROG. It is not fast enough to record traces at a speed of 10 Hz, which is the repetition rate of the laser. A faster computer and controller is needed to achieve 10 Hz readout rate and to show traces at the same speed. Many systems exist on the market, but the signal to noise ratio generally drops as the readout rate is increased. If it is enough to view the traces, the readout speed can be increased by binning the CCD chip. For more detailed studies of the trace, binning will reduce the resolution too much.

All FROG types use a signal created through an autocorrelation. In the autocorrelation process, only a part of the cross section of the pulses interact, which makes it impossible for the autocorrelation signal to contain complete information of the pulse shearness. An improvement could be obtained if no cylindrical lens is used in the TG FROG setup. Then three autocorrelation signals are created which all have a delay axes in different directions (Chapter 7.C). The three signals together would give more information about shearness, but to gain this information the spectrometer and CCD camera would have to be turned so that the input slit is along each separate delay axis. It is an impractical procedure, and the situation would not be much improved.

8.6 Acknowledgements

When doing this diploma work I have had the opportunity to work with an excellent personel, that has in every way let me develop my personal skills and acquire experience. My supervisor, Claes-Göran Wahlström, is a great source of inspiration and knowledge, and I think it is very few granted to have such guidance. The excellent laser system specialist, Anders Persson, has not even once told me he is in a hurry or out of time. His theoretical and practical help and pieces of advise were invaluable in many situations. I have had the pleasure to discuss autocorrelators in theory and practice with Matthias Grätz, who is a never ending source of ideas and a great support in times of need. Professor Sune Svanberg, who is an inspirer for the whole division, has supported me throughout the work. Krishna Mohan, Baozhu Luo and Stefan Kröll have helped me with the theory of nonlinear optics whenever needed. Computer problems were solved by Bertil Hermansson and broken things were quickly repaired by Åke Bergqvist, the technician. I would also like to thank the ever smiling secretaries Laila Lewin and Marie Holmdahl-Svensson. My caring girlfriend Helen Gillgren has stoically put up with my irregular working hours and supported my work in every way.

Concluding, I am very grateful for the time I have spent in the inspiring environment of the atomic physics division in Lund.

9 References

- [1] G. Taft, A. Rundquist, M. M. Murnane, I. P. Christov, H. C. Kapteyn, K. W. DeLong, D. N. Fittinghoff, M. A. Krumbügel, J. N. Sweetser, R. Trebino, *Measurement of 10-fs laser pulses*, IEEE journal of selected topics in quantum electronics, Vol. 2, No. 3, pp 575-584, 1996
- [2] J.T. Fourkas, L.Dhar, K.A. Nelson, *Spatially encoded, single-shot ultrafast spectroscopies*, JOSA B, Vol. 12, No. 1, pp. 155-165, 1995
- [3] L. Dhar, J.T. Fourkas, K.A. Nelson, *Pulse-length-limited ultrafast pump-probe spectroscopy in a single laser shot*, Optics letters, Vol. 19, No. 9, pp. 643-645, 1994
- [4] H.P. Weber, *Method for pulsewidth measurement of ultrashort light pulses generated by phase locked lasers using nonlinear optics*, Journal of applied physics, Vol. 38, No 5, pp. 2231-2234, 1967
- [5] J. Jansky, G. Corradi, R.N. Gyuzalian, *On a possibility of analysing the temporal characteristics of short light pulses*, Optics Communications, Vol, 23, No. 3, pp. 293-298, 1977
- [6] R.N. Gyuzalian, S.B. Sogomonian, Z.Gy. Horvath, *Background-free measurement of time behaviour of an individual picosecond laser pulse*, Optics Communications, Vol. 29, No. 2, pp. 239-242, 1979
- [7] C. Yan, J.C. Diels, *Amplitude and phase recording of ultrashort pulses*, JOSA B, Vol. 8, pp 1259-1263, 1991
- [8] K. Naganuma, K. Mogi, H. Yamada, *General method for ultrashort light pulse chirp measurement*, IEEE Journal of quantum electronics, Vol. 25, pp. 1225-1233, 1989
- [9] T. Kobayashi, F.-C. Guo, A. Morimoto, T. Sueta, Y. Cho, *Novel method of waveform evaluation of ultrashort optical pulses*, Ultrafast Phenomena IV, D.H. Auston, K.B. Eiseenthal, Springer-Verlag, pp.93-95, 1984
- [10] J.L.A. Chilla, O.E. Martinez, *Direct determination of the amplitude and the phase of femtosecond lighth pulses*, Optics Letters, Vol. 16, No. 1, pp. 39-41, 1991
- [11] J.L.A. Chilla, O.E. Martinez, *Frequency-domain phase measurement of ultrashort light pulses. Effect of noise*, Optics Communications, Vol. 89, pp. 434-440, 1992
- [12] J.L.A. Chilla, O.E. Martinez, *Analysis of a method of phase measurement of ultrashort pulses in the frequency domain*, IEEE Journal of quantum electronics, Vol. 27, pp. 1228-1235, 1991
- [13] A. Sullivan, W.E. White, K.C. Chu, J.P. Heritage, K.W. DeLong, R. Trebino, *Quantitative investigation of optical phasemeasuring techniques for ultrashort pulse lasers*, JOSA B, Vol. 13, No. 9, pp. 1965-1978, 1996
- [14] R. Trebino. K.W. DeLong, D.N. Fittinghoff, J.N. Sweetser, M.A. Krumbügel, B.A. Richman, D.J. Kane, *Measuring ultrashort laser pulses in the time-frequency domain using frequency-resolved optical gating*, Rev. Sci. Intrum., Vol. 68, No. 9, pp. 3277-3295, 1997
- [15] D.J. Kane, R. Trebino, *Characterization of arbitrary femtosecond pulses using frequency-resolved optical gating*, IEEE Journal of Quantum electronics, Vol. 29, No. 2, pp. 571-579, 1993
- [16] John N. Sweetser, David N. Fittinghoff and Rick Trebino, *Transient-grating frequency-resolved optical gating*, Optics Letters, Vol. 22, No. 8, pp. 519-521, 1997
- [17] Sandia National Laboratories, *FROG information from Sandia WEB pages*, <http://www.ca.sandia.gov/ultrafrog/index.html>
- [18] A.M. Levine, E. Özizmir, R.Trebino, C.C. Hayden, A.M. Johnson, K.L. Tokuda, *Induced-grating autocorrelation of ultrashort pulses in a slowly responding medium*, JOSA B, Vol. 11, No. 9, pp. 1609-1618, 1994

- [19] K.W. DeLong, R. Trebino, D.J. Kane, *A comparison of ultrashort-pulse frequency-resolved-optical-gating traces for three common beam geometries*, JOSA, Vol. 11, No. 9, pp. 1595-1608, 1994
- [20] R. Trebino, K.W. DeLong, D.N. Fittinghoff, J.N. Sweetser, M. Krumbuegel, J. Bowie, G. Taft, A. Rundquist, M.M. Murnane, A.C. Kapteyn, *Measurement of the intensity and phase of ultrashort pulses using frequency-resolved optical gating*, Ultrafast Processes in Spectroscopy, pp. 603-606, 1996
- [21] D.J. Kane, R. Trebino, *Single-shot measurement of the intensity and phase of an arbitrary ultrashort pulse by using frequency-resolved optical gating*, Optics Letters, Vol. 18, No. 10, pp. 823-825, 1993
- [22] J. Paye, M. Ramaswamy, J.G. Fujimoto, E.P. Ippen, *Measurement of the amplitude and phase of ultrashort light pulses from spectrally resolved autocorrelation*, Optics Letters, Vol. 18, No. 22, pp. 1946-1948, 1993
- [23] E. T. J. Nibbering, M. A. Franco, B. S. Prade, G. Grillon, J.-P. Chambaret and A. Mysyrowicz, *Spectral determination of the amplitude and the phase of intense ultrashort optical pulses*, JOSA B, Vol. 13, No. 2, pp. 317-329, 1996
- [24] B.S. Prade, J.M Schins, E.T.J. Nibbering, M.A. Franco, A. Mysyrowicz, *A simple method for the determination of the intensity and phase of ultrashort optical pulses*, Optics Communications 113, pp. 79-84, 1994
- [25] M.A. Franco, J.-F. Ripoche, H.R. Lange, J.P. Chambaret, P. Rousseau, B.S. Prade, A. Mysyrowicz, *How to measure femtosecond pulses*, To appear in the proceedings of the international conference on Superstrong Fields in Plasmas, Villa Monastero, Varenna, Italy, 1997
- [26] D.J. Kane, A.J. Taylor, R. Trebino, K.W. DeLong, *Single-shot measurement of the intensity and phase of a femtosecond UV laser pulse with frequency-resolved optical gating*, Optics Letters, Vol. 19, No. 14, pp. 1061-1063, 1994
- [27] S. Svanberg, J. Larsson, A. Persson, C.-G. Wahlström, *Lund high-power laser facility - systems and first results*, Physica Scripta, Vol. 49, pp. 187-197, 1994
- [28] H. Schulz, H. Schüler, T. Engers, D. von der Linde, *Measurement of intense ultraviolet subpicosecond pulses using degenerate four-wave mixing*, IEEE Journal of quantum electronics, Vol. 25, No 12, pp. 2580-2585, 1989
- [29] Landolt-Börnstein, *Numerical data and functional relationships in science and technology*, Group III: Crystal and solid state physics, Vol. 11, 1979
- [30] Landolt-Börnstein, *Numerical data and functional relationships in science and technology*, Group III: Crystal and solid state physics, Vol. 18, 1984
- [31] R.W. Boyd, *Nonlinear optics*, Academic Press, Inc., 1997
- [32] Y.R. Shen, *The principles of nonlinear optics*, John Wiley & Sons, Inc., 1984
- [33] G. Szabó, Z. Bor, A. Müller, *Phase-sensitive single-pulse autocorrelator for ultrashort laser pulses*, Optics letters, Vol. 13, No. 9, 1988
- [34] R. Trebino, D.J. Kane, *Using phase retrieval to measure the intensity and phase of ultrashort pulses: frequency resolved optical gating*, JOSA A, Vol. 10, No. 5, pp. 1101-1111, 1993
- [35] K.W. DeLong, D.N. Fittinghoff, R. Trebino, *Practical issues in ultrashort-laser-pulse measurement using frequency-resolved optical gating*, IEEE Journal of quantum electronics, Vol. 32, No. 7, pp. 1253-1264, 1996
- [36] D.N. Fittinghoff, K.W. DeLong, R. Trebino, C.L. Ladera, *Noise sensitivity in frequency-resolved optical-gating measurements of ultrashort pulses*, JOSA B, Vol. 12, No. 10, pp. 1955-1967, 1995
- [37] T. Tsang, M.A. Krumbügel, K.W. DeLong, D.N. Fittinghoff, R. Trebino, *Frequency-resolved optical-gating measurements of ultrashort pulses using surface third-harmonic generation*, Optics Letters, Vol. 21, 1996

- [38] L. Will, P. Nickles, M. Schnuerer, M. Kalashnikov, W. Sandner, *Compact FROG system useful for measurement of multiterawatt laser pulses*, Optics Communications, Vol 132, pp. 101-106, 1996
- [39] A. Brun, P. Georges, G. Le Saux, F. Salin, *Single-shot characterization of ultrashort light pulses*, Physics D: Applied Physics, Vol. 24, pp. 1225-1233, 1991
- [40] A. Khyzniak, V. Kondilenko, Y. Kucherov, S. Lesnik, S. Odoulov, M. Soskin, *Phase conjugation by degenerate forward four-wave mixing*, JOSA A, Vol. 1, No. 2, pp. 169-175, 1984
- [41] V. Kondilenko, S. Odolov, M. Soskin, *Degenerate forward four-wave mixing in LiNbO₃*, Ferroelectrics Letters, Vol. 1, pp. 19-26, 1983
- [42] P. Günter, J.-P. Hulgnard, *Photorefractive materials and their applications I - fundamental phenomena*, Topics in applied physics vol 61, Springer-Verlag
- [43] P. Günter, J.-P. Hulgnard, *Photorefractive materials and their applications II - survey of applications*, Topics in applied physics vol 62, Springer-Verlag
- [44] J. N. Sweetser, *private communication*, December 1997
- [45] B. Luther-Davies, M. Samoc, J. Swiatkiewicz, A. Samoc, M. Woodruff, R. Trebino and K.W. DeLong, *Diagnostics of femtosecond laser pulses using films of poly(p-phenylenevinylene)*, <http://laserspark.anu.edu.au/frogoc/frogoc.html>
- [46] B. Luther-Davies, M. Samoc, J. Swiatkiewicz, A. Samoc, M. Woodruff, R. Trebino and K.W. DeLong, *Diagnostics of femtosecond laser pulses using films of poly(p-phenylenevinylene) (PPV)*, <http://laserspark.anu.edu.au/FROG/FROGPortland.html>
- [47] Z. Bor, Z. Gogolak, G. Szabo, *Femtosecond-resolution pulse-front distortion measurement by time-of-flight interferometry*, Optics letters, Vol. 14, No. 16, pp. 862-864, 1989
- [48] P.M.W. French, *The generation of ultrashort laser pulses*, Reports on Progress in Physics, Vol. 58, pp. 169-267, 1995
- [49] K.L. Sala, G.A. Kenney-Wallace, G.E. Hall, *CW autocorrelation measurements of picosecond laser pulses*, IEEE Journal of Quantum electronics, Vol. QE-16, No. 9, pp. 990-996, 1980
- [50] A.E. Siegman, *Lasers*, University Science Books, 1986
- [51] J. Swartling, J. Dahlberg, *Propagering av ultrakorta laserpulser genom optiska komponenter*, Project report in Optical Quantum Mechanics course at LTH by S. Kröll

Appendix A Derivation of relation between pulse duration and width of autocorrelation curve

Gaussian pulses

A pulse with a gaussian intensity profile,

$$I(t) = I_0 \cdot e^{-2at^2}$$

$$a = 2 \cdot \ln(2) \cdot \frac{1}{\tau_{FWHM}^2} \quad (\text{A.1})$$

Multiple shot

The relation between the width of the autocorrelation curve and laser pulse duration is easily derived for a n :th order slow autocorrelation signal with one pulse delayed [48,49]. The expression for the detected signal is now a crosscorrelation, $W_n(\tau)$,

$$W_n(\tau) = \frac{\int_{-\infty}^{\infty} I^{n-1}(t) \cdot I(t+\tau) \cdot dt}{\int_{-\infty}^{\infty} I^n(t) \cdot dt}$$

The intensity has a gaussian profile.

$$W_n(\tau) = \frac{\int_{-\infty}^{\infty} I_0 \cdot e^{-2(n-1)at^2} \cdot I_0 \cdot e^{-a(t+\tau)^2} \cdot dt}{\int_{-\infty}^{\infty} I_0^2 \cdot e^{-2na \cdot t^2} \cdot dt} = \frac{\int_{-\infty}^{\infty} e^{-2a \cdot ((n-1)t^2 + (t+\tau)^2)} \cdot dt}{\int_{-\infty}^{\infty} e^{-2na \cdot t^2} \cdot dt} =$$

$$= \frac{\int_{-\infty}^{\infty} e^{-2a \cdot ((n-1)t^2 + (t+\tau)^2)} \cdot dt}{\sqrt{\frac{\pi}{2 \cdot n \cdot a}}} = \frac{\int_{-\infty}^{\infty} e^{-2na \cdot \left(\left(t + \frac{\tau}{n} \right)^2 + \frac{\tau^2}{n} - \frac{\tau^2}{n^2} \right)} \cdot dt}{\sqrt{\frac{\pi}{2 \cdot n \cdot a}}} = \frac{\int_{-\infty}^{\infty} e^{-2na \cdot \left(t + \frac{\tau}{n} \right)^2} \cdot dt}{\sqrt{\frac{\pi}{2 \cdot n \cdot a}}} \cdot e^{-2a \cdot \frac{n-1}{n} \tau^2} =$$

$$= \frac{\sqrt{\frac{\pi}{2 \cdot n \cdot a}}}{\sqrt{\frac{\pi}{2 \cdot n \cdot a}}} \cdot e^{-2a \cdot \frac{n-1}{n} \tau^2} = e^{-4 \cdot \ln(2) \cdot \left(\frac{\tau}{\sqrt{\frac{n}{n-1}} \cdot \tau_{\text{intensity FWHM}}} \right)^2}$$

In the last expression there is a relationship between τ_{delay} (the FWHM of the autocorrelation curve) and τ_{FWHM} for a n :th order slow autocorrelation,

$$\tau_{FWHM} = \tau_{\text{delay}} \cdot \sqrt{\frac{n-1}{n}} \quad (\text{A.3})$$

For any second order autocorrelator it means that

$$\tau_{FWHM} = \frac{\tau_{\text{delay}}}{\sqrt{2}}, \quad (\text{A.4})$$

and for any third order autocorrelator,

$$\tau_{FWHM} = \tau_{\text{delay}} \cdot \sqrt{\frac{2}{3}} \approx \frac{\tau_{\text{delay}}}{1.22} \quad (\text{A.5})$$

Naturally, this result applies also if the sign of τ is changed or, as for PG FROG, the intensity profile of the delayed profile is squared rather than the one not delayed as above.

Single shot

The same relations as above hold for single shot autocorrelators. The only difference is that the delay is realized in a different way, namely through the interpulse angle (Ch. 3.3.2). Delay smearing (Ch. 5.3.4), frequency-width effects (Ch. 5.3.8) and errors alignment may however increase τ_{delay} . If no correction is made for this, the laser pulse duration will be overestimated.

Sech pulses

A pulse with a sech^2 intensity profile,

$$I(t) = I_0 \cdot \text{sech}^2(a \cdot t) = \frac{I_0}{\left(\frac{e^{a \cdot t} + e^{-a \cdot t}}{2}\right)^2} \quad (\text{A.6})$$

$$a = 2 \cdot 0.881374 \cdot \frac{1}{\tau_{\text{FWHM}}}$$

Multiple shot

For a third order autocorrelation curve, the same expression as for the gaussian pulse shape in (A.5) is derived numerically.

$$\tau_{\text{FWHM}} = \frac{\tau_{\text{delay}}}{1.27} \quad (\text{A.7})$$

The uncertainty is about 1%.

Single shot

The broadening effects discussed for single shot measurements with gaussian pulses are independent of the pulse shape so they apply for sech^2 pulses also.

Appendix B Additional nonlinear processes in the pulse alignment procedure

When the KDP crystal is used and the alignment is perfect something extraordinary happens. On a paper blocking all pulse coming from the crystal eleven spots are visible (Fig. B.1). All the spots originates from nonlinear processes in the crystal. A quick calculation reveals that at least up to sixth order processes occur in the crystal. Table B.1 shows what kind of process that correspond to a certain spot in terms of wave vectors [31,32]. Not all possible processes are included, only those experimentally verified. ω

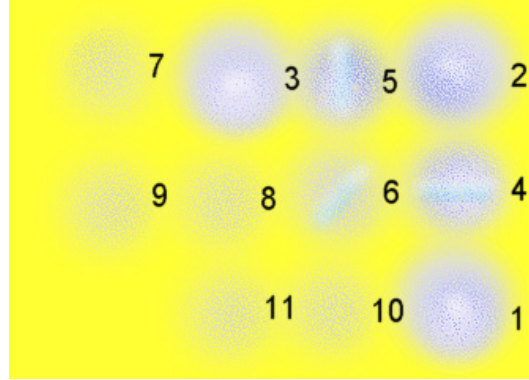


Figure B.1. Additional light spots appear in the alignment procedure due to additional, nonlinear processes in the KDP crystal.

Table B.1. Nonlinear processes corresponding to each light spot.

Spot number	Nonlinear process	Signal frequency	Nonlinear process	Signal frequency
1	\bar{k}_1	ω	$2\bar{k}_1$	2ω
2	\bar{k}_2	ω	$2\bar{k}_2$	2ω
3	\bar{k}_3	ω	$2\bar{k}_3$	2ω
4	$\bar{k}_1 + \bar{k}_2$	2ω		
5	$\bar{k}_2 + \bar{k}_3$	2ω		
6	$\bar{k}_1 + \bar{k}_3$	2ω		
7	$3\bar{k}_3 - \bar{k}_2$	2ω		
8	$2\bar{k}_3 + \bar{k}_1 - \bar{k}_2$	2ω		
9	$3\bar{k}_3 + \bar{k}_1 - 2\bar{k}_2$	2ω		
10	$2\bar{k}_1 + \bar{k}_3 - \bar{k}_2$	2ω		
11	$\bar{k}_1 + \bar{k}_3 - \bar{k}_2$	ω	$2\bar{k}_1 + 2\bar{k}_3 - 2\bar{k}_2$	2ω

Appendix C Calibration of wavelength

The wavelength calibration is a straight forward procedure. When the CCD camera and the spectrometer are fixed in position, a calibration lamp with proper wavelengths are placed in front of the input slit on the spectrometer. In all cases the light intensity must be damped with filters to avoid saturation of the CCD chip.

The laser to be diagnosed has a central wavelength of 800 nm. Since the emission lines are known through tables, it is relatively easy to turn the grating in the spectrometer so that 800 nm lies in the middle of the wavelength axis. Thereafter all the different wavelength lines are identified and the position on the chip is noted. Theoretically it is enough with two identified lines, but many more is identified to be sure that the wavelength scale is correct. To verify the calibration some spectra is recorded of the laser pulse. The widths of the spectra agree well with the pulse duration.

For reference the calibration curves are included. Rubidium (Rb) has only two strong wavelength lines close to 800 nm (Fig. H.1). From a table it is known which of the lines that should be the strongest. Therefore it is possible to determine in which direction the wavelength increases. The calibration curve for Argon (Ar) is given in Figure H.2.

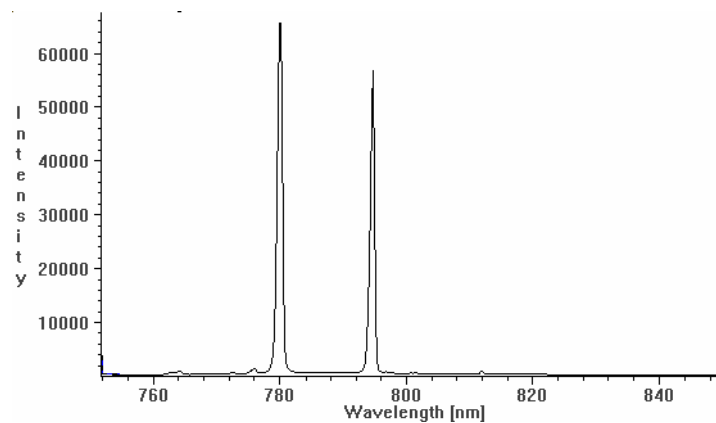


Figure H.1. The calibration curve for Rubidium.

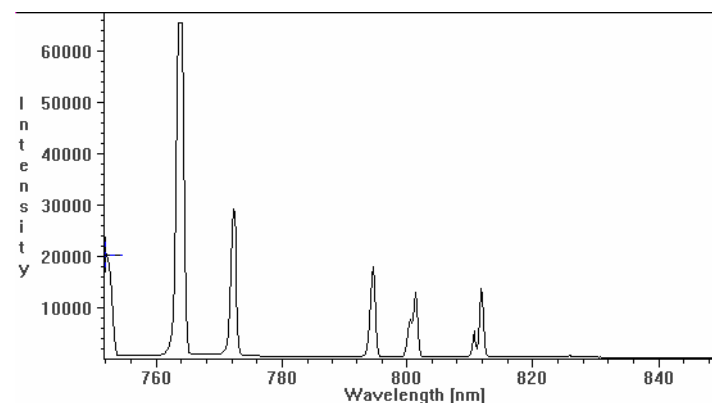


Figure H.2. The calibration curve for Argon.

Appendix D Calibration of delay

It is of great importance to have full control of the delay axis in the FROG-trace. The program FROG 1.5 uses a delay dispersion (femtoseconds per pixel) in its calculations. If an incorrect dispersion is entered the resulting E-field and spectrum will also be incorrect.

Theoretically, it is possible to calculate the delay dispersion in the interaction region (Ch. 5.3.2). The FROG signal passes through both a spectrometer and an objective before the CCD-chip records it. From the position of the camera and the objective settings the magnification from the image plane at the spectrometer to the CCD-chip should be about 0.46. It is known also that the spectrometer magnifies the delay axis by a factor of 1.2 (Ch. 6.4). The magnification could be calculated, but to be sure an experimental calibration was done. The 120 μm input slit is used in the spectrometer and the 50 μm slit is mounted perpendicular to the other on a vertical translator. The 50 μm slit is placed close to the input slit of the spectrometer. By shining through the 50 μm slit with an argon-lamp and translating it 1.00 mm between each recording it is possible to calculate the actual magnification,

$$m_2 = \frac{122.7}{98.85} \cdot 0.490 = 0.608. \quad (\text{D.1})$$

Appendix E Resolution of the delay-axis for TG FROG

When viewing infinitely short overlapping pulses with infinite cross sections in two dimensions, it is easy to derive an expression for the delay resolution (Fig. E.1). The position of one pulse is described by

$$y = v \cdot t, \quad (\text{E.1})$$

and the other two pulses are described by

$$y \cdot \cos(\beta) - x \cdot \sin(\beta) = v \cdot t. \quad (\text{E.2})$$

Eq. (E.2) is differentiated with respect to time, and x is solved for,

$$\frac{dx}{dt} = \frac{\frac{dy}{dt} \cdot \cos(\beta) - v}{\sin(\beta)}. \quad (\text{E.3})$$

Inserting the derivative with respect to time of (E.1) into (E.3) yields an expression for the speed of the point of crossing,

$$\frac{dx}{dt} = \frac{v \cdot \cos(\beta) - v}{\sin(\beta)} = -v \cdot \tan\left(\frac{\beta}{2}\right). \quad (\text{E.4})$$

If the y -axis is perpendicular to the surfaces of the nonlinear medium with thickness d , it takes $\Delta t = \frac{d}{v}$ for the point of crossing to traverse it. During this time, the point of crossing moves

$$|\Delta x| = d \cdot \tan\left(\frac{\beta}{2}\right) \quad (\text{E.5})$$

along the delay axis. This corresponds to a delay shift of

$$\Delta \tau = d \cdot \tan\left(\frac{\beta}{2}\right) \cdot T = \frac{n_{\text{medium}} \cdot d}{c_0} \cdot \tan\left(\frac{\beta}{2}\right) \cdot \tan(\beta) \approx \frac{n_{\text{medium}} \cdot d \cdot \beta^2}{2c_0}. \quad (\text{E.6})$$

The delay shift in the present TG FROG setup is 11 fs for $d=1$ mm, and 6 fs for $d=0.55$ mm if the refractive index is 1.51 and $\beta=3.73^\circ$. The actual TG process takes place in three dimensions so the true delay resolution will always be smaller than the one derived here. How much smaller depends on the width of the input slit of the spectrometer.

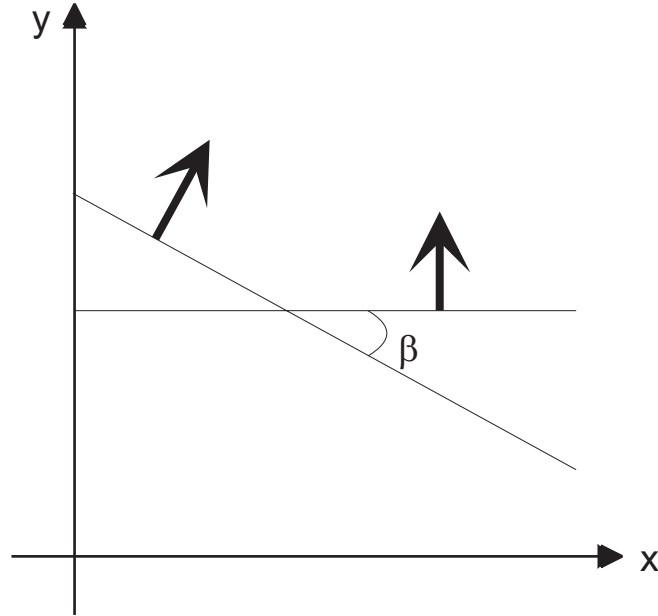


Figure E.1. Two infinitely short and infinitely wide pulses overlapping and propagating in different directions.

Appendix F The PG FROG trace

There are some facts concerning the PG FROG trace that should be revealed. First, the marginals of the FROG trace will be examined. The expression for the signal is well known by now,

$$E_{\text{FROG}}^{\text{PG}}(t, \tau) \propto E(t) \cdot |E(t - \tau)|^2 \propto e^{-(a-ib)t^2 - 2a(t-\tau)^2} \cdot e^{i\omega_0 t} \quad (\text{F.1})$$

Eq (F.1) is fourier transformed, squared and rewritten to

$$\left| \hat{E}_{\text{FROG}}^{\text{PG}}(\omega, \tau) \right|^2 \propto e^{-2\frac{6a^3+2ab^2}{9a^2+b^2} \cdot \tau^2} \cdot e^{-\frac{1}{29a^2+b^2} \cdot 3a \cdot (\omega - \omega_0)^2} \cdot e^{-\frac{4ab}{9a^2+b^2} \cdot \tau \cdot (\omega - \omega_0)} \quad (\text{F.2})$$

If the linear chirp, b , is zero and (F.2) is integrated with respect to frequency to get the delay marginal, M_τ , the result is the same as for a third order cross correlation with gaussian pulses and without chirp (App. A),

$$M_\tau^{\text{PG}}(\tau) = \int_{-\infty}^{\infty} \left| \hat{E}_{\text{FROG}}^{\text{PG}}(\omega, \tau) \right|^2 \cdot d\omega \propto e^{-\frac{4}{3} \cdot \tau^2} \quad (\text{F.3})$$

It is possible to show that the PG delay marginal is proportional to a third order cross correlation function for any pulse form [19],

$$M_\tau^{\text{PG}}(\tau) \propto \int_{-\infty}^{\infty} I^2(t) \cdot I(t - \tau) \cdot dt \quad (\text{F.4})$$

The pulse duration is therefore easily determined with help of the pulse duration relation for third order autocorrelators, derived in Appendix A. The PG frequency marginal can also be derived [19],

$$M_{\omega}^{PG}(\omega) \propto I(\omega) \cdot F\left(\int_{-\infty}^{\infty} I(t) \cdot I(t-\tau) \cdot dt\right), \quad (\text{F.5})$$

which is a product between the laser pulse spectrum fourier transform of the second order intensity autocorrelation.

It would be interesting to understand how linear chirp changes the FROG trace. If the mean frequency of (F.2) is calculated, an expression is derived that tells how the mean frequency, or mean wavelength, varies with delay, τ ,

$$\langle \omega \rangle = \frac{\int_{-\infty}^{\infty} \omega \cdot |\hat{E}_{\text{FROG}}^{\text{SD}}(\omega, \tau)|^2 \cdot d\omega}{\int_{-\infty}^{\infty} |\hat{E}_{\text{FROG}}^{\text{SD}}(\omega, \tau)|^2 \cdot d\omega} = \omega_0 - \frac{4b}{3} \cdot \tau \Rightarrow, \quad (\text{F.6.a})$$

$$\langle \lambda \rangle = \lambda_0 - \frac{2b \cdot \lambda_0^2}{3\pi \cdot c_0} \cdot \tau \approx \lambda_0 - 453 \cdot 10^{-24} \cdot b \cdot \tau, \quad \lambda_0 = 800 \text{ nm}. \quad (\text{F.6.b})$$

Now it is possible to estimate the amount of linear chirp by some simple calculations. Figure F.1 is a FROG trace as recorded in the experimental setup. The line indicates the approximate linear function of eq. (F.6.b). From the line, the linear chirp is estimated to $130 \cdot 10^{24} \text{ s}^{-2}$.

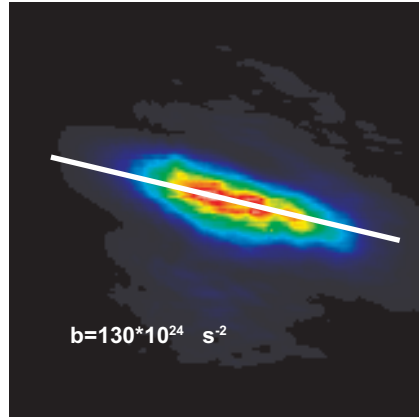


Figure F.1. Experimental TG FROG trace at grating translator position 3.81, where the pulse should be approximately free of chirp.

Appendix G Chirp due to pulse propagation

The laser pulse can change a lot when it propagates from the laser laboratory to an experiment. One reason is that the refractive index of air depends on the frequency, so called Group Velocity Dispersion (GVD), and the instant intensity, so called Self Phase Modulation (SPM). An expression will be derived to calculate the acquired linear chirp, b ,

as a function of the distance the pulse propagates. The B-integral, $\frac{2\pi}{\lambda_0} \cdot \int_0^L \gamma \cdot I_0(z) \cdot dz$, which quantize the SPM only, will be calculated for comparison reasons [50]. The refractive index depends on intensity,

$$n(t) = n_0 + \gamma \cdot I(t). \quad (\text{G.1})$$

The GVD will not be evident until n_0 is assumed to be a function of frequency. The phase to be added to the pulse is

$$\begin{aligned} \varphi(t) &= -\frac{2\pi}{\lambda_0} n(t) \cdot z = -\frac{2\pi}{\lambda_0} (n_0 + \gamma \cdot I(t)) \cdot z = \\ &= -\left(\frac{2\pi}{\lambda_0} n_0 + \frac{2\pi\gamma \cdot I(t)}{\lambda_0} \right) \cdot z = -\left(k + \frac{2\pi\gamma \cdot I(t)}{\lambda_0} \right) \cdot z \end{aligned} \quad (\text{G.2})$$

This phase is added to the expression for a gaussian pulse,

$$E(t) \propto e^{-(a-ib)t^2} \cdot e^{i\omega_0 t} \cdot e^{i\varphi(t)} = e^{-(a-ib)t^2} \cdot e^{i\omega_0 t} \cdot e^{-i\left(k + \frac{2\pi\gamma \cdot I(t)}{\lambda_0}\right) \cdot z}. \quad (\text{G.3})$$

To simplify matters, the intensity is written as a MacLaurin series,

$$I(t) = I_0 e^{-2a \cdot t^2} \approx I_0 (1 - a \cdot t^2), \quad (\text{G.4})$$

where I_0 is the peak intensity of the pulse. Eq. (G.4) is inserted into (G.3),

$$E(t) \propto e^{-\left(a - i\left(b + \frac{2\pi\gamma \cdot I_0}{\lambda_0} \cdot a \cdot z\right)\right) \cdot t^2} \cdot e^{i\omega_0 t} \cdot e^{-i\left(k + \frac{2\pi\gamma \cdot I_0}{\lambda_0}\right) \cdot z} \approx e^{-\left(a - i\left(b + \frac{2\pi\gamma \cdot I_0}{\lambda_0} \cdot a \cdot z\right)\right) \cdot t^2} \cdot e^{i\omega_0 t} \cdot e^{-ik \cdot z} \quad (\text{G.5})$$

and (G.5) is fourier transformed,

$$\hat{E}(\omega) \propto e^{-\frac{1}{4}\left(a - i\left(b + \frac{2\pi\gamma \cdot I_0}{\lambda_0} \cdot a \cdot z\right)\right)^{-1} \cdot (\omega - \omega_0)^2} \cdot e^{-ik(\omega)z}. \quad (\text{G.6})$$

The variable $k(\omega)$ is expanded around ω_0 and all terms except the second order term, the GVD term, are dropped,

$$\begin{aligned} \hat{E}(\omega) &\propto e^{-\frac{1}{4}\left(a - i\left(b + \frac{2\pi\gamma \cdot I_0}{\lambda_0} \cdot a \cdot z\right)\right)^{-1} \cdot (\omega - \omega_0)^2} \cdot e^{-i\frac{d^2 k(\omega_0)}{2 d\omega^2} \cdot z \cdot (\omega - \omega_0)^2} = \\ &= e^{-\frac{1}{4}\left(\left(a - i\left(b + \frac{2\pi\gamma \cdot I_0}{\lambda_0} \cdot a \cdot z\right)\right)^{-1} + i\frac{d^2 k(\omega_0)}{d\omega^2} \cdot 2z\right) \cdot (\omega - \omega_0)^2} \end{aligned} \quad (\text{G.7})$$

The inverse fourier transform of (G.7) is

$$E(t) \propto e^{-\left(\left(a - i\left(b + \frac{2\pi\gamma \cdot I_0}{\lambda_0} \cdot a \cdot z\right)\right)^{-1} + i\frac{d^2 k(\omega_0)}{d\omega^2} \cdot 2z\right)^{-1} \cdot t^2}. \quad (\text{G.8})$$

Eq. (G.8) is simplified into

$$E(t) \propto e^{-(A-ib)t^2}, \quad (\text{G.9})$$

if the variables

$$\begin{aligned}
K_1 &= b + \frac{2\pi\gamma \cdot I_0}{\lambda_0} \cdot a \cdot z \\
K_2 &= \frac{d^2k(\omega_0)}{d\omega^2} \cdot 2z \\
K_3 &= K_1 + K_2 \cdot (a^2 + K_1^2) \\
A &= \frac{a^2 + K_1^2}{a^2 + K_3^2} \cdot a \\
B &= \frac{(a^2 + K_1^2) \cdot K_3}{a^2 + K_3^2}
\end{aligned} \tag{G.10}$$

are used. The constant, A , is calculated to see if the pulse duration changes. Any reasonable conditions for the present experimental setup leads to a maximum pulse prolongation of about 10% according to (G.10). The total chirp, B , varies a lot, though, and one finds that it is approximately proportional to z , γ and I_0 . It is therefore possible, with a small error, to sum the chirp for different parts of the pulse path to a final chirp. This is good to know when one has some millimeters of glass and some meters of air and perhaps a telescope in the path.

The values of the material constants at 800 nm are $\frac{d^2k_{air}(w_0)}{d\omega^2} = 2.112 \cdot 10^{-29} \text{ s}^2/\text{m}$, $\frac{d^2k_{BK7}(w_0)}{d\omega^2} = 4.483 \cdot 10^{-26} \text{ s}^2/\text{m}$, $\gamma_{air} = 0.47 \cdot 10^{-22} \text{ m}^2/\text{W}$ and $\gamma_{BK7} \approx 1 \cdot 10^{-19}$ [31,51]. In the present setup, the total energy of one pulse is typically 1.6 mJ, the FWHM cross section of the pulses is 24 mm and the pulse duration used in the calculations is 110 fs. If the pulse is Gaussian the peak intensity becomes $I_0 = 23 \text{ TW}/\text{m}^2$. The calculated chirp magnitudes are acquired mainly through SPM (a good $\frac{3}{4}$ of it). The magnitude of the chirp correspond to the experimental conditions given above, but the calculation method should be approximately correct for any super intense laser pulse. For the above pulses, the chirp from travel in 10 m air is $b = 20 \cdot 10^{24} \text{ s}^{-2}$ (B-integral=0.09) and from 1 mm of BK7 glass, $b = 4 \cdot 10^{24} \text{ s}^{-2}$ (B-integral=0.02). If the pulse is compressed in a 5:1 telescope and split into three equal parts, each part will get additional chirp. From 2 m of air, $b = 20 \cdot 10^{24} \text{ s}^{-2}$ (B-integral=0.14) and from 2 mm of BK7, $b = 43 \cdot 10^{24} \text{ s}^{-2}$ (B-integral=0.3). Totally each of the three pulses will have a linear chirp of about $b = 90 \cdot 10^{24} \text{ s}^{-2}$ (B-integral=0.54) when they enter the nonlinear medium in the TG FROG. If the pulses are focused down to 50 μm and passes through 0.5 mm of BK7 the chirp magnitude will finally be $b = 190 \cdot 10^{24} \text{ s}^{-2}$ (B-integral=16). The B-integral is well above the critical value of π . It is, however, difficult to say how much of this chirp that the FROG signals will reflect, because they are created simultaneously as the pulses are changing. The corresponding chirp (which also includes GVD) is easily detected by the present TG FROG according to Appendix F. It is possible to remove the GVD part of the chirp by pulse manipulations, but the SPM part can never be totally removed.